AD 709 736

DETERMINATION OF CONSTITUTIVE RELATIONS FROM PLANE WAVE EXPERIMENTS

Richard Fowles

WSU SDL 70-01

April 1970

DETERMINATION OF CONSTITUTIVE RELATIONS FROM PLANE WAVE EXPERIMENTS[†]

Richard Fowles[*]
Shock Dynamics Laboratory, Washington State University

ABSTRACT

Recent developments in experimental methods for measuring the characteristics of plane compression waves are reviewed, and analytical methods for inferring constitutive relations from measured wave profiles are discussed. A general method, requiring only pressure or particle velocity measurements, is proposed that is applicable to arbitrary waves in which equilibrium or steady state may not obtain. A summary of current knowledge of constitutive relations obtained from plane wave experiments is also presented.

[†]Basis of a talk given Tuesday, August 26, 1969, 1:30 p.m., at Symposium 2, "Characterization of the Dynamic Behavior of Materials," at the A.S.M.E. Applied Mechanics Western Conference in Albuquerque, New Mexico, August 25-27, 1969.

[*]Current address: Physics International Co., San Leandro, California.

BLANK PAGE

DETERMINATION OF CONSTITUTIVE RELATIONS FROM PLANE WAVE EXPERIMENTS

I. INTRODUCTION

The behavior of solids under impact loading at stresses above the linear range of material response has been a subject of study since about 1872.[1] The earliest work and much subsequent work has been done with experimental arrangements that produce conditions of one-dimensional stress, i.e. rod experiments.

Since the Second World War increasing attention has been given to plane waves, in which the strain is accurately one-dimensional. Because of this strain condition deformation of the material takes place under superimposed hydrostatic pressures and, at the higher stress levels, at elevated temperatures resulting largely from adiabatic compression.

The most distinctive feature of plane wave compression, however, is the existence of shock fronts. In these fronts the strain rates can be exceedingly high - in many cases exceeding the resolution capabilities of the recording instrumentation. Nonequilibrium states necessarily exist even in a steady-state shock. Thus, a relatively complete time-dependent and temperature-dependent constitutive relation is required to predict plane-wave propagation; by the same token a wide range of information about material properties can be obtained from plane-wave experiments.

The complexities of shock experiments are mitigated considerably by the accuracy with which the one-dimensional strain boundary condition can be produced. In rod experiments the corresponding one-dimensional stress condition is less easy to verify and has been a difficult and annoying problem in experiments near the impacted end.

The constitutive relation obtained from shock experiments is, however, that pertinent to one-dimensional strain, and it is probably unreasonable to expect that from experiments in this geometry alone one can infer a completely general constitutive relation. Nearly all experimental techniques measure only the stress component in the direction of propagation. The component in the direction tangential to the wavefront can usually only be inferred. Where hydrostatic compression data are available comparison with shock data permits the shear stress behind the shock front to be deduced. Alternatively, measurement of the states obtaining in the relief of stress (via a rarefaction wave) from a shocked state provides much information about the yield stress under shock conditions.

To a considerable degree shock waves have been used as experimental tools for the study of high pressure physical phenomena and several reviews have appeared in recent years which emphasize that aspect of shock wave physics.[2-6] For these studies stress anisotropy and stress relaxation effects are undesired complications and are frequently ignored. Such effects are not negligible at lower pressures or where wave propagation is the principal interest.

In this article we focus on the experimental aspects of nonlinear plane wave propagation in solids. Our attention is thus directed principally to stresses between the elastic yield point and stresses one or two orders of magnitude higher. To predict wave propagation in this regime requires a time-dependent constitutive relation for one-dimensional strain. The converse of this problem, namely how to deduce constitutive relations from observations of wave propagation, is the central theme of the paper. An earlier review of this aspect of shock wave physics has been given by Karnes.[7]

The remainder of this section is devoted to a brief description of some of the most important features of the shock transition. Section II reviews methods for producing plane waves, and describes recent developments in recording techniques for observing wave behavior.

In Section III analytical methods for extracting information about constitutive relations from measured wave profiles are discussed. In that section I propose a rigorous method for the reduction of pressure-time data that does not require the usual assumptions of steady state or equilibrium, isentropic flow.* Section IV presents a review of current knowledge of constitutive relations derived from plane-wave experiments.

A. Some Properties of Shock Waves

1. Jump Conditions

By "shock front" one means a compressive (usually) wave front which is steady. That is, a shock front transforms the mechanical and thermodynamic state of the material to one of higher stress, density, energy and mass velocity. The initial and final states are equilibrium states but the transition region, or shock front, necessarily involves non-equilibrium states. Because the transition region is steady, no mass, momentum, or energy accumulates within it and conservation laws can be applied to relate the initial and final states. These conservation laws, called the Rankine-Hugoniot jump conditions, can be written:[8]

$$V_1/V_o = 1 - [(u_1-u_o)/(U-u_o)] \tag{1}$$

$$P_1 - P_o = \rho_o(U-u_o)(u_1-u_o) \tag{2}$$

$$E_1 - E_o = [(P_1+P_o)/2](V_o - V_1) \tag{3}$$

In these equations V ($= \rho^{-1}$) is specific volume, P is the component of normal stress in the direction of shock propagation (not necessarily an equilibrium stress), E is specific internal energy, u is mass velocity, and U is the shock front velocity. Subscripts o refer to the state

*While this paper was in preparation I learned that Mr. Roger Williams had made the same discovery independently.[37]

ahead of the shock, while subscripts 1 refer to the shocked state.

It is readily shown that these equations imply that the entropy of the shocked state is higher than that of the initial state.[2,8] The locus of equilibrium states given by Eq. (3) is, for a given material in a given initial state, a unique function called the Hugoniot, or R-H curve, which therefore lies above the isentrope through the initial state. A complete equation of state for a material can be characterized by a family of R-H curves centered on different initial states.

Note that the components of normal stress parallel to the shock front do not enter the equations directly. They influence the shock only through the equation of state, which properly should be termed the equilibrium constitutive relation for one-dimensional compression.

The jump conditions apply not only to the equilibrium end states but throughout the transition region since each portion of the front is also steady. Equations (1) and (2) can be combined to give:

$$U - u_o = V_o \sqrt{(P_1-P_o)/(V_o-V_1)} \qquad (4)$$

Since all parts of the wave travel with the same velocity, $U - u_o$, with respect to the undisturbed material, the locus of P, V, E states in the transition must lie on the straight line joining the initial and end states in the P-V plane. This line is called the Rayleigh line. (Figure 1.)

The difference between the Rayleigh line and the R-H curve at a given volume is approximately the non-equilibrium stress obtaining in the transition region and is primarily responsible for the entropy production.* If the material is treated as a viscous fluid, the steady-state shape of the shock front can be derived by relating the non-equilibrium stress to the stress rate or strain rate.[9,10]

2. Stability of Shock Waves

*The thermal part of this difference is normally negligible in solids.

In solids a single shock front is frequently unstable and a compressive wave propagates as two or more shock fronts. The stability criterion is derived by assuming the shock to consist of two fronts and comparing their relative speeds.[2]

Assume that the first shock, travelling with velocity U_B in laboratory coordinates, transforms the state to $P_B - P_A$, $u_B - u_A$. Its velocity with respect to the material behind it is then $U_B - u_B$. The velocity of the second shock is U_C in laboratory coordinates, and $U_C - u_B$ with respect to the material ahead of it. The final state is P_C, V_C.

Employing the jump conditions, Eqs. (1) and (2), these velocities can be written

$$U_B - u_B = V_B \sqrt{(P_B-P_A)/(V_A-V_B)}$$

$$U_C - u_B = V_B \sqrt{(P_C-P_B)/(V_B-V_C)}$$

If the assumed second shock travels faster than the first a single front is stable. Thus, the condition for stability is:

$$(P_C-P_B)/(V_B-V_C) > (P_B-P_A)/(V_A-V_B)^*$$

Graphically this means that the Rayleigh line joining point P_B, V_B with P_C, V_C is steeper (more negative) than that joining P_B, V_B with P_A, V_A. (Figure 2.)

A cusp in the P-V curve as indicated at point B in Figure 2 occurs in the majority of solids at the elastic yield point. Because the strain is one-dimensional, shear stresses are developed by a plane wave. In an elastic solid the relation is:[11]

---

*Although this derivation is not entirely rigorous, more detailed examination shows the result to be correct.

$$\tau = [(1-2\nu)/(2(1-\nu))]P$$

where τ is the shear stress and ν is Poisson's ratio. Clearly, as P increases so does τ until the material yields. The elastic portion of the P-V curve has slope,

$$-(dP/dV) = K + (4/3)\mu,$$

where K is the bulk modulus and μ the shear modulus. In the plastic region above the yield point the slope is reduced to (neglecting work hardening):

$$-(dP/dV) = K$$

Accordingly there is a range of shock amplitudes for which the stability criterion is not satisfied. Since K increases with pressure, however, the unstable region is bounded at higher pressures (Point D in Fig. 2) as well as at the elastic limit.

Instability can also result from phase transformations. The isothermal volume discontinuity of a first-order phase change frequently corresponds to a cusp in the R-H curve and the consequent separation of shock fronts is very suitable for experimentally detecting the transition and measuring its pressure.

3. Reflections at Interfaces

For plane waves the interaction with a boundary of different shock impedance is characterized by continuity of the stress normal to the boundary and the mass velocity. For this reason it is convenient to consider the relations between stress and particle velocity obtaining in shock transitions and in rarefactions.

The shock velocity can be eliminated from Eqs. (1) and (2) to give

$$u_1 - u_0 = \pm\sqrt{(P_1-P_0)(V_0-V_1)} \qquad (5)$$

From this relation a family of curves can be plotted in the P-u plane, once an equation of state is given, that represents the locus of equilibrium P, u states attainable by a shock transition from a given initial state. Except for the end states the transition states do not lie on this curve but on the straight line joining the end states, analogous to the Rayleigh line in the P-V plane. Those curves with positive slope are pertinent to forward-facing shock fronts (i.e. shock fronts travelling in the +x direction); those with negative slope pertain to backward-facing waves.

For rarefaction waves, which reduce the stress and accelerate the material in the direction opposite to that of propagation, the relation between stress and mass velocity is given by the Riemann integral*:[8]

$$u_1 - u_0 = \pm \int(dP/\rho c) \qquad (6)$$

where c is the local sound speed.

This relation can also be represented in the P-u plane as a family of curves, and, as for shocks, forward-facing waves are described by the curves with positive slope, while backward-facing waves are described by those with negative slope.

Where the effect on the R-H curve of the entropy change inherent in the shock transition is small the two families of curves are the same and no distinction need be made. All transitions from a given initial state must lie on one of the two curves passing through that state.

For example, consider the reflection of a forward-facing shock in material A at an interface with material B, assumed to possess smaller shock impedance than A. (Figure 3.) The initial shock is represented by P_1, u_1 and lies on the P-u curve of material A centered on (0,0).

---

*This result is a consequence of assuming constant entropy and therefore does not hold across shock fronts.

Reflection of the shock at the boundary produces a backward-facing rarefaction in A and a forward-facing shock in B. The common state at the interface must lie on the intersection of the appropriate curves centered respectively on (P_1, u_1) and $(0,0)$, i.e. the final state is (P_2, u_2).

If material B were a free surface the reflected rarefaction would have carried material A to zero pressure and the free-surface velocity, u_{fs}. Note that if the p-u curves for shocks and rarefactions are the same the free-surface velocity is just twice the particle velocity prior to reflection. This result is frequently used to infer particle velocities from measured free-surface velocities for well-behaved materials.

The P-u plane is an indispensable tool for qualitative or semi-quantitative analysis of complex wave interactions and a set of curves for known materials is to be found in virtually all experimental laboratories.

II. EXPERIMENTAL TECHNIQUES

A. Production of Plane Stress Waves

The principal tool for producing plane stress waves for the study of constitutive relations is the single stage compressed gas gun. For precisely controlled impacts these devices are at present unsurpassed.[12-14]

Existing guns vary considerably in their design; nevertheless there are certain common features. They are all smooth bore, usually having been drilled to close tolerances from a solid forging or casting. They use compressed nitrogen or helium as the driving gas, pressurized up to about 6000 psi. Substantially improved performance would result from the use of hydrogen, but handling and safety problems have discouraged use of this gas. Siegel has given an exhaustive treatment of the gas dynamics in guns of this type.[15]

The projectile diameters vary from 2-1/2" to 6"; the barrel lengths from about 10' to 100'. The velocities achieved vary from about

0.1 mm/μs to 1.5 mm/μs. Higher velocities are exceedingly difficult to reach in a single stage gun, except that use of hydrogen could increase the velocities to about 2 mm/μs. Velocities lower than 0.1 mm/μs can be achieved but non-reproducible frictional losses tend to make the projectile velocities erratic in this range. Table I shows some pressures produced by impact at 1.5 mm/μs.

The barrels are evacuated ahead of the projectile to prevent a gas cushion from distorting the wave shape. Hard vacuums are evidently not necessary; Barker was able to detect no effect at residual gas pressures below 0.6 torr in the Sandia 3 meter gun.[16] Impact with the target usually takes place an inch or two in front of the muzzle to provide space for expansion of the projectile while still maintaining a maximum degree of alignment of projectile and target.

The tilt angle between the projectile and target must be precisely controlled if true plane waves are to be produced, particularly at lower impact velocities. The angle of the wavefront with respect to the target surface is frequently an order of magnitude or more larger than the misorientation of the projectile with the target because of the large difference between wave velocity and impact velocity.

Large tilt not only produces two-dimensional flow but reduces the time-resolution of the recording instrumentation. Thus if the recording gauge has finite dimensions in the plane parallel to the impact surface, the time resolution achieved may be controlled by the time required for the wave front to sweep across the gauge.

Ir practice angular misorientations of a few tenths of a milliradian are commonly achieved. A tilt of this magnitude would typically result in a time resolution, for a gauge whose lateral dimensions are 1/4 inch, of about 5 nanoseconds. Since this is comparable to the resolution of typical fast oscilloscopes the desirability of small tilt is obvious.

The recoil of guns of this type can be difficult to contend with while maintaining the precise orientations required. Where the target is mounted rigidly to the barrel, vibrations can precede the projectile and cause anomalous signals. A convenient solution incorporated into the gun of the Shock Dynamics Laboratory at Washington State University is to allow the gun to move freely while holding the target rigidly on a separate support.[14] The motion of the gun greatly reduces the recoil forces and does not seem to adversely affect the tilt provided the barrel is maintained nearly torque-free. A drawing of the WSU gas gun is shown in Fig. 4. This gun has a 4" bore, a length of 46', and operates on nitrogen or helium to 6000 psi. It is typical of many guns of this type.

Guns that use gunpowder as the propellant are in limited use. Although they can be shorter for a given velocity, and therefore are less expensive, the problems of cleanliness and high recoil forces make them somewhat less desirable for studies of constitutive relations.

For very high velocities, two-stage, light-gas guns can be used.[17,18] The velocities of these guns can reach 8 mm/μs; however, the projectile diameters are generally less than two inches. This is a severe restriction since useful one-dimensional information is obtained from the target only before the effects of free lateral surfaces influence the wave shape. Accordingly only simple measurements of shock velocity, from which equation of state points are determined, have been attempted with these guns.

High explosives have been used to produce plane waves and are useful for extending the pressure range available from single-stage guns. These systems utilize a plane-wave lens to produce a plane detonation wave at the target interface.[2] In some cases useful information has been obtained from two-dimensional steady state waves produced by a running detonation.[11]

In addition to producing higher pressures, explosives are convenient in that precise synchronization with recording instruments can be achieved. This is important when high speed cameras are used because they frequently record only over a small time interval and cannot be triggered by the event to be observed.

Disadvantages to explosives are that the plane waves produced are less precisely controlled than is the case with guns. Moreover, a continuous range of impact pressures is very difficult to achieve. For these reasons explosives are most frequently used for equation of state measurements and for the study of other high pressure physical phenomena.

Electron beams and lasers are also beginning to be used for the production of plane waves.[19,20] These produce stress waves through thermoelastic coupling when radiant energy is absorbed in the target material in times short compared to the transit time of rarefaction waves.

Electron beams provide much higher energy densities; with electron energies in the range 0.2 to 5.0 mev the maximum fluence (energy per cm^2) varies between about 35 and 300 cal/cm^2. The corresponding stress pulses produced depend on the absorbing material but are typically ten to several hundred ns in duration, and attain peak stress amplitudes up to about 100 kbar. The area over which the flux is reasonably uniform is a few square centimeters.[19]

Lasers operated in the pulse mode give comparable pulse durations and irradiated areas, but deliver total energies one to two orders of magnitude less than do electron beams.

These methods are most useful when it is desired to observe stress wave propagation under high temperature conditions or when very short pulse durations are desirable.

B. Measurement Techniques

Parameters which are directly pertinent to a description of plane stress wave propagation are the normal stress component acting across a plane perpendicular to the direction of propagation, the density or strain, the internal energy, the mass velocity, and, in general, two phase velocities. The existence of two phase velocities is not widely recognized and indeed for steady shock fronts or isentropic rarefactions the two velocities are the same. In general, however, they are distinct, as is shown in Section III.

Three independent relations expressing conservation of mass, momentum, and energy can be written relating the above parameters; Eqs. (1)-(3) are those relations for the special case of steady flow. Consequently, three measurements are required in order to determine the state. The normal stress components parallel to the wavefront are not directly involved. They can be inferred under certain conditions, however, by comparing the compression and relief paths in the P-V plane or when a hydrostat is known independently.

The measurements which can be most accurately made at present include the normal stress component and the free-surface velocity, which can be related in many cases to the mass velocity. For some materials mass velocity can be measured directly. From measurements of these quantities at two or more locations in the sample one or both of the phase velocities can be obtained.

A variety of optical techniques using high speed cameras have been invented and used successfully to record surface velocities (and wave velocities). These include argon flash gaps, inclined mirrors, moving images, and optical lever techniques. The precision of these methods is usually about 1% in wave velocity and 5% in free surface velocity. The time resolution is generally about 10 ns.

Electrical methods are also in wide use and include electrical shorting pins, inclined resistance wires, and capacitor microphones. These also measure free-surface velocities with a precision comparable to that of optical methods.

A transducer technique in wide use at present is the quartz gage, which measures the pressure at the interface between the sample and a disc of x-cut quartz plated on both flat surfaces.[21] At stresses up to about 25 kilobars the current developed by the piezoelectric polarization of the quartz is proportional to the stress at the quartz-sample interface. Useful results have been obtained at higher stress levels but 50 kilobars is about the upper limit. It has high inherent time resolution and is convenient to use.

All of the above techniques suffer from a common drawback; namely, the observations are made at an interface at which there is usually an impedance mis-match. Consequently, in order to infer the character of the undisturbed wave requires an impedance-matching analysis similar in principle to that mentioned in Section I. This analysis cannot be performed rigorously without knowledge of the constitutive relation of the sample, although useful information can be extracted by making some reasonable approximations and with subsequent iteration. For some materials such as aluminum the quartz gage is a reasonably good impedance match and the analysis is less sensitive to uncertainties in the constitutive relation of the sample.

Detailed descriptions of the above techniques have appeared in several review articles in recent years and the reader is referred to those for a more thorough presentation.[2,22,23] The remainder of this section is devoted to more recent developments; these include piezoresistive gauges, electromagnetic velocity gauges, sapphire gauges, and laser interferometry.

1. Piezoresistive Gauges

Manganin wire was first used as a pressure transducer in hydrostatic apparatus by Bridgman in 1911.[24] It is desirable for this purpose because it exhibits a positive pressure coefficient of resistance and at the same time a very small temperature coefficient.

In 1964, Bernstein and Keough,[25] and Fuller and Price,[26] reported experiments in which a fine manganin wire was imbedded in an epoxy disc. The disc was used much as is a quartz gage; it was placed against the free surface of a sample and the change in resistance monitored as the pressure pulse, transmitted into the epoxy by an initial pulse in the sample, passed over the wire. (Figure 5.) These experiments established that the fractional change in resistance is linearly proportional to pressure up to about 300 kbar.

Numerous dynamic experiments have yielded pressure coefficients in the range[27]

$$(1/R)(\Delta R/\Delta P) = 2.0 \text{ to } 2.9 \times 10^{-3}/\text{kbar}$$

The statically determined value is 2.6×10^{-3}/kbar.

These discrepancies have not yet been fully resolved; the values seem to depend on the supplier of the manganin and/or the calibration technique. For this reason some investigators use manganin gauges at present primarily as interpolation gauges between pressures established independently.[28] For commercial manganin a value near 2.9×10^{-3} seems to be most widely observed; little or no temperature dependence has been observed so that the calibration should not depend on the material in which the manganin is imbedded. There is some indication that there is a hysteresis effect so that the coefficient may be different when measuring the compression part of a pulse than when measuring the rarefaction portion. It is uncertain whether this effect is real, however, or what physical mechanisms might be responsible.

In spite of these difficulties it seems reasonable to expect that, as development proceeds, a reproducible gauge with a well-determined coefficient can be fabricated.

Because of impedance mismatches between the sample and the insulating material in which the gauge is imbedded, the gauge used in this mode has the same limitations mentioned above when an undisturbed wave profile is desired.

More recently, experiments have been performed in which the manganin is imbedded directly into the sample material.[27] In this mode a relatively undisturbed record of the shape of the pressure pulse is obtained. A variety of thin elements have been developed for this purpose. They are typically 0.001" or less in thickness and frequently are in the shape of a grid in order to increase the resistance of the active part of

the gauge while maintaining small lateral dimensions.[29] It is desirable of course to keep the thickness as small as possible in order to increase the inherent time resolution, which is dependent on the reverberation time through the thickness. Small lateral dimensions are also desirable to minimize losses in time resolution due to tilt of the wavefront with respect to the plane of the gauge.

An example of one such grid is shown in Fig. 6. This gauge was photoetched from manganin sheet rolled to 0.00075" thickness. The lateral dimensions of the active element are 1/8" and the resistance is about 1.5 ohms. This gauge has four terminals in order to use a bridge method for recording the resistance changes. With the bridge method and a constant current power supply the effects of stretching of the current or voltage leads due to edge effects is minimized.

When the sample to be investigated is an insulator a gauge of this type can be inserted directly into the sample with only a very thin layer of cement to fill the voids between the grid elements. If the sample is a conductor, however, thin insulation must be added to prevent premature shorting. Insulating materials such as mylar, mica, glass and Lucalox have been employed. Of these, Lucalox is attractive because it has high electrical breakdown potential, and it has high shock impedance so that the impedance match with metals is improved over, say, mylar.[27] Because of its low compressibility the change in capacity between the element and the sample is also minimized. A disadvantage is that fabrication of thin films is difficult; plasma sprayed films are one possible solution.[29]

The time resolution of these gauges when used in metal samples is somewhat poorer than the time resolution of quartz gauges, for example, principally because of the insulation thickness. If the total gauge thickness including insulation is several thousandths of an inch and several reverberations of the pressure pulse are required to establish equilibrium between the gauge and the sample, the time resolution can be of the order of 30-50 nanoseconds.

Recording durations of gauges of this type are normally several microseconds, and for laboratory use are generally larger than the times for which one-dimensional flow can be maintained. Careful treatment of the leads is important for longer recording times since shearing of these is the usual cause of premature failure.

Experiments with vapor plated manganin grids and with other materials such as calcium, lithium and ytterbium show considerable promise for improving the low pressure sensitivity of gauges of this type.[30] Calcium, for example, exhibits a pressure coefficient roughly ten times as great as manganin at pressures at least up to 28 kbar. However, it has much higher temperature sensitivity.

An interesting variation on this method has been reported by Bernstein, et al.[31] They have used two manganin grids oriented respectively in planes parallel and perpendicular to the direction of propagation. Each grid measures the stress component normal to its plane so that the difference in signals is a measure of the effective yield stress.

2. Electromagnetic Velocity Gauges

When the sample to be studied is an insulator an electromagnetic technique can be used to measure mass velocities directly. This technique was first used to measure detonation parameters in explosives. Its use in inert solids was first reported by Dremin who used it to determine the behavior of glass under shock loading.[32] Ainsworth and Sullivan have also reported extensive measurements on rocks up to 30 kbar.[33]

The idea is that a fine wire or foil imbedded in an insulator develops a potential difference when it moves in a magnetic field. Thus, to the extent that the foil motion is the same as that of the insulator, a measurement of the voltage across the wire can be related to the mass velocity of the insulator.

The experiment is shown schematically in Fig. 7. If the magnetic field strength is B, and ℓ is the length of the foil perpendicular to both B and to the mass velocity, u, Faraday's law of induction reduces to:

$$\mathcal{E} = -(\partial/\partial t) \int B \cdot dA = B\ell u$$

where $\mathcal{E}$ is the emf. If we insert typical values into this expression we find

$$\mathcal{E} = 500 \text{ gauss} \times 1 \text{ cm} \times 10^5 \text{ cm/sec} = 0.5 \text{ volt.}$$

A field strength of this magnitude is readily attainable and yields an easily measurable signal at mass velocities of interest.

It is perhaps surprising, in view of the simplicity of the method, that it has not been more widely used. It cannot be used, of course, on conducting samples because eddy currents induced into the sample would distort the magnetic field.

One might suspect that the polarization field induced into an insulator, by virtue of the dielectric constant of the insulator, would distort the electric field in the wire or the magnetic field itself and influence the measurement. Detailed examination of these effects, however, shows them to be negligible.[34]

Ainsworth and Sullivan state that the method is useful up to about 30 kbar. However, it is not clear why such a limitation need be imposed; Dremin reports measurements up to about 400 kbar in glass.

When used with guns or explosives precautions must, of course, be taken to prevent the motion of the projectile or explosive gases from distorting the magnetic field.

The precision reported by Dremin is approximately 3%. As with manganin gauges thin foils are desirable to achieve high time resolution.

3. Sapphire Gauges

Some recent work has been devoted to developing sapphire as a transducer.[35] It is used in similar fashion to the quartz gauge, but depends for its operation on the change in capacitance due to the change in dielectric constant and to the reduced electrode separation resulting from shock compression.

The current developed by the gauge is a function of the mass velocity of the impacted surface; the relation is linear at low velocities and is expressed as:

$$i(t) = (VAU/\ell^2)\,[\gamma + (\varepsilon_i/U)]\,u(t), \qquad 0 < t < \ell/U$$

In this expression i(t) is the observed current, V is the initial applied voltage (of the order of 2 kilovolts), A is area of the disc, ℓ is the thickness of the disc, U the shock velocity, ε_i and γ are the unstressed permittivity and the rate of change of permittivity with mass velocity.

At higher impact velocities the relation becomes nonlinear, but can be readily expressed in terms of measurable constants of the material.

Sapphire in the 60° orientation seems to be usable at impact stresses up to 100 kbar in the sapphire. Because its shock impedance is relatively high it provides a reasonably good impedance-match to heavier metals, such as iron. The principal disadvantage is the short recording time available from reasonable crystal thicknesses, caused by the high shock speed. This time is typically 0.25 μsec.

Other materials, such as ruby and Z-cut quartz have also been examined as possible gauges of this type.[35] The lower yield stress of ruby, however, limits its usefulness to stresses below about 40 kbar. Z-cut quartz is not suitable at present because it exhibits internal conduction and noise.

4. Laser Interferometry

Interferometric measurements provide the highest time and space resolution currently attainable. For these methods a laser is not only convenient as a coherent light source but is necessary in order to achieve the requisite high light intensities.

Two schemes have been reported; both of them were developed by Barker.[16,36] The first of these uses the laser in a conventional Michelson interferometer arrangement and is shown schematically in Fig. 8. The portion of the laser beam reflected from the mirror surface of the specimen is compared with that reflected from a stationary mirror. Interferometric fringes are thus formed, each of which corresponds to a displacement of the surface of one-half wavelength and the spatial resolution is therefore of the order of 0.3 micron.

The laser beam is focused on the specimen mirror surface in order to minimize the effect of projectile tilt. This surface can either be a polished free surface, in which case the problems of relating free-surface velocity to mass velocity are the same as in many of the techniques mentioned above, or it may be a mirror surface plated on an internal surface of a transparent specimen. In this case a direct measure of mass velocity is obtained. In either case impact stresses must be limited to those for which the mirror retains its integrity.

When measuring the displacement of an internal surface a correction is required for the change of index of refraction of the shocked "window". The relation that best fits current data is the Gladstone-Dale formula:[36]

$$d\rho/\rho = dn/(n-1)$$

where ρ is density and n is the index of refraction.

The uncertainty introduced by lack of complete independent knowledge of the density in the shock (which is one of the parameters one

wishes to determine) does not produce serious errors because the density changes involved are usually small.

The principal disadvantage to the technique described above is that the spatial resolution is generally too high. Consequently, for mass velocities greater than about 0.2 mm/μs the fringe frequency exceeds the capabilities of current recording systems (approx. 600 MHz).

By means of a clever modification of the above technique the space and time resolution can be adjusted over a wide range; moreover, the fringe frequency is proportional to the acceleration of the mirror rather than to its velocity.[36] Each fringe then corresponds to a velocity increment of predetermined magnitude.

In this modification, the "velocity interferometer technique," interference fringes are formed by superposition of two portions of the laser beam reflected from the specimen surface at different times. The earlier signal is delayed a predetermined amount with respect to the later signal. The arrangement is shown in Fig. 9.

The operation can be understood by referring to Fig. 10. If the time through the delay leg is $\tau = t_2 - t_1$ and the distance travelled by the mirror surface in that time is S, then

$$S = \bar{u}\tau$$

where $\bar{u}$ is the average surface velocity over the interval τ. The signal reaching the photomultiplier at time $(t_2 + t_c)$, where t_c is constant, is thus composed of the signal reflected at time t_2 plus that reflected at time t_1. If the velocity of the surface is constant in time the separation of the surfaces, $S = x(t_2) - x(t_1)$, is constant and the fringe frequency is zero. If the surface accelerates, however, fringes will appear at the rate

$$(\lambda/2)(dn/dt) = (dS/dt) = \tau(d\bar{u}/dt)$$

or, since n is zero when $\bar{u}$ is zero,

$$\bar{u}(t) = (\lambda/2\tau)\, n(t)$$

where n is the number of fringes counted.

The resolution of the system is controlled by the delay leg. For very small delays the number of fringes per velocity change is small and the resolution in velocity is correspondingly reduced. With a typical delay leg of 10 nsec and a wavelength of 6328 Å, the coefficient,

$$d\bar{u}/dn = 31.64 \text{ m/sec/fringe.}$$

The time resolution, on the other hand, is equal to the delay time. This can be seen by observing that the technique effectively measures the separation of two surfaces displaced in time by τ. Consequently, a constant velocity, for example, will not be observed as constant until both surfaces move with constant velocity, i.e. until the specimen surface has travelled with constant velocity for a time τ.

The balance to be struck between these two resolutions depends on the experiment. The values indicated above, however, show that reasonably good resolution of both time and velocity are attainable.

Although laser methods are somewhat restricted in application, the high time resolutions attainable and the accuracy with which they can be calibrated makes them essential tools in the experimentalist's repertoire.

III. INTERPRETATION OF EXPERIMENTS

As indicated above current experimental techniques in general provide measurements of pressure-time or velocity-time histories at locations fixed with respect to the material, i.e. in Lagrangian coordinates. If the measurement is made at a boundary where the shock impedance changes, as in

free-surface measurements or quartz gauge measurements, the recorded data are characteristic of two superimposed waves - the incident wave plus the wave reflected from the boundary. To separate the effects of each wave requires knowledge of the constitutive relation (in general, time-dependent) of the material. Thus, in principle the derivation of a constitutive relation from such measurements requires prior knowledge of the constitutive relation and the analysis is somewhat circular.

Valuable information can nevertheless be obtained through a series of successive approximations. The question of convergence of these methods does not seem to have been treated theoretically, but frequently the results are not sensitive to small errors in the assumptions. Some of the techniques do not suffer from this uncertainty - notably piezoresistive pressure transducers and electromagnetic velocity gauges. However, these techniques have other limitations so that most of the techniques in use are complementary.

Once stress-time and/or velocity-time data are obtained for the undisturbed wave in the sample the question arises how to interpret the data to derive a one-dimensional strain constitutive relation. If the compressive part of the wave is steady the jump conditions (Eqs. (1)-(3)) are valid and the analysis is straightforward. In the rarefaction portion of the wave one usually assumes that the states, while not steady, are nevertheless equilibrium states and that the stress is a function of the density only, i.e. the flow is assumed isentropic. The jump conditions can then be applied incrementally to yield a stress-density "isentropic" relation for the rarefaction part of the wave. The Riemann integral, Eq. (6), is just the integrated momentum jump condition (Eq. (2)).

Unfortunately these assumptions are frequently not met in an experiment and the interpretation is accordingly not rigorous.

An alternative means of interpretation is to assume a constitutive relation and attempt to reproduce the experimental observations by trial and error using a computer. This method is not only expensive but offers no guarantee of uniqueness.

A. Arbitrary Waves

It is not difficult to show what kinds of measurements are necessary and how they should be interpreted in order to deduce directly the stress, density, and energy states obtaining in an arbitrary wave. This method requires no assumptions about the form of the constitutive relation, steadiness of the wave, or extent to which the states are equilibrium states.

The equations expressing conservation of mass, momentum and energy are, in Lagrangian coordinates:[38]

$$(\partial V/\partial t) - V_0(\partial u/\partial h) = 0 \tag{7}$$

$$(\partial u/\partial t) + V_0(\partial P/\partial h) = 0 \tag{8}$$

$$(\partial E/\partial t) + (P/\rho_0)(\partial u/\partial h) = 0 \tag{9}$$

In these equations h is the initial (undisturbed) coordinate of a particle, ρ is density (ρ_0 is initial density), P is the stress component in the direction of propagation, u is mass velocity, and E is specific internal energy.

These equations are generally valid. The only restriction is that heat flow has been assumed negligible in Eq. (9). Thus, within that restriction, the equations apply equally to compressive or release waves and are independent of any assumption about the constitutive relation.

We define two phase velocities associated with the wave as follows:

$$c_u = (\partial h/\partial t)_u$$

and

$$c_p = (\partial h/\partial t)_p$$

since h and t are the independent variables, P = P(h,t) and u = u(h,t), and,

$$dP = (\partial P/\partial t)dt + (\partial P/\partial h)dh,$$

also,

$$du = (\partial u/\partial t)dt + (\partial u/\partial h)dh.$$

Thus,

$$c_p = -\frac{\partial P/\partial t}{\partial P/\partial h} \tag{10}$$

$$c_u = -\frac{\partial u/\partial t}{\partial u/\partial h} \tag{11}$$

Combining Eqs. (7) and (11):

$$(\rho_o/\rho^2)(\partial\rho/\partial t) - (1/c_u)(\partial u/\partial t) = 0$$

or

$$(\rho_o/\rho^2)d\rho - (1/c_u)du = 0, \quad \text{along } h = \text{const.}$$

Combining Eqs. (8) and (10):

$$(\partial u/\partial t) - (1/\rho_o c_p)(\partial P/\partial t) = 0$$

or

$$dP = \rho_o c_p\, du, \quad \text{along } h = \text{const.}$$

Similarly:

$$dE = (P/\rho_o c_u)du, \quad \text{along } h = \text{const.}$$

Summarizing, we have

$$dV = -du/\rho_o c_u \tag{12}$$

$$dP = \rho_o c_p du \qquad \text{(along } h = \text{const)} \qquad (13)$$

$$dE = (P/\rho_o c_u)du \qquad (14)$$

These equations can be applied incrementally to observed wave shapes to relate velocities to stress, density, and energy. Note that Eqs. (12) and (13) are equivalent to the ordinary jump conditions in differential form (in Lagrangian coordinates) except that different phase velocities must be used. Only for steady state waves, discontinuous shock fronts or isentropic simple waves will these velocities be equal in general.

The mass velocity can be eliminated from Eqs. (12) and (13) to give the stress-density relation:

$$dP/d\rho = (\rho_o^2/\rho^2)c_p c_u, \qquad \text{along } h = \text{const.} \qquad (15)$$

Clearly, this reduces to the acoustic relation whenever the phase velocity $c = c_p = c_u$. Similarly, we can write:

$$dE = (PdP/\rho_o^2 c_u c_p) \qquad \text{along } h = \text{const.} \qquad (16)$$

Implementation of this method in experiments requires, at a minimum, measurements of pressure-time profiles at more than one location in the specimen. From these the velocities c_p can be obtained and mass velocity profiles deduced from Eq. (13). Thence, c_u values can be obtained and the density and energy calculated. Simultaneous particle-velocity measurements would be valuable and might enhance the precision but are not essential. Particle velocity measurements alone, without pressure measurements, would require an iterative procedure to deduce P and c_p and, although less convenient, could be used.

The data obtained are values of one-dimensional stress, density, and internal energy for each part of the wave as it progresses through the material. From this information one can fit various models to obtain a

general relation for stress as a function of strain, energy, strain-rate, history, etc. The stress components parallel to the wavefront might also be inferred from a variety of such measurements or from independent hydrostatic data.

The relation between the phase velocities can be derived from

$$c_p - c_u = (\partial h/\partial t)_p - (\partial h/\partial t)_u$$

$$= (\partial h/\partial t)_p - [(\partial h/\partial t)_p + (\partial h/\partial p)_t (\partial P/\partial t)_u]$$

$$= c_p \frac{(\partial P/\partial t)_u}{(\partial P/\partial t)_h}$$

or

$$1 - c_u/c_p = \frac{(\partial P/\partial t)_u}{(\partial P/\partial t)_h} ;$$

Similarly, (17)

$$1 - c_p/c_u = \frac{(\partial u/\partial t)_p}{(\partial u/\partial t)_h}$$

Consequently, the phase velocities will be equal whenever the stress is a function of velocity only, or when the wavefront represents a discontinuity in stress or mass velocity.

There are two cases when stress is a function of velocity only - steady flow and isentropic simple waves. This is shown in the following two sections. We can conclude immediately, however, that whenever $P = P(u)$ the lines of constant phase are straight lines in the h,t plane. That is, $c_u = c_p = c_p(P)$ from Eq. (13), and $(\partial c_p/\partial h)_p = 0$.

B. Steady State

For steady state shock fronts the phase velocity c_p is the same for all parts of the wave and Eq. (13) can be integrated to give the usual momentum jump condition

$$P - P_o = \rho_o(U-u_o)(u-u_o)$$

where c_p has been replaced by the shock velocity with respect to material coordinates, $U-u_o$. Further, since P is a function of u only, we have:

$$c_u = \frac{du}{dP}\left(\frac{\partial P/\partial t}{du/dP}\right)\frac{\partial P}{\partial h} = c_p$$

Thus, Eq. (12) becomes

$$d\rho = [\rho^2/\rho_o(U-u_o)]du$$

Integrating yields the continuity jump condition

$$1 - \rho_o/\rho = (u-u_o)/(U-u_o)$$

The stress-volume curve is seen to be a straight line joining the end states (Rayleigh line) for, integrating Eq. (15) yields,

$$U - u_o = V_o\sqrt{(P-P_o)/(V_o-V)} = \text{const.}$$

Finally, Eq. (16) yields the Rankine-Hugoniot relation:

$$E - E_o = (1/2)(P+P_o)(V_o-V)$$

Note that this derivation does not require that the states be equilibrium states (except insofar as steady state implies equilibrium end states). Moreover, if the shock front is considered to be a discontinuity then $c_p = c_u$ and the jump conditions hold even if the flow behind the wave is unsteady.

C. Isentropic Flow in Fluids

The development of non-linear wave propagation theory in fluids relies heavily on the method of characteristics.[8] This method, in turn, depends on the assumption that the flow is everywhere particle-isentropic and that, therefore, all states are equilibrium states.

If to Eqs. (7) and (8) we add the relations:

$$(\partial S/\partial t)_h = 0 \tag{18}$$

and

$$P = P(\rho, S) \tag{19}$$

where S is entropy, we can write:

$$(\partial P/\partial \rho)_S = a^2 \quad \text{on } h = \text{const.},$$

where a is the sound speed with respect to spatial (Eulerian) coordinates. This relation allows us to eliminate the derivative in ρ from Eq. (7):

$$(\rho_o/\rho^2)(\partial \rho/\partial P)(\partial P/\partial t) + \partial u/\partial h = 0$$

or

$$\partial P/\partial t + (\rho^2 a^2/\rho_o)(\partial u/\partial h) = 0 \tag{20}$$

Multiplying Eq. (8) by a,

$$\rho a(\partial u/\partial t) + (\rho a/\rho_o)(\partial P/\partial h) = 0 \tag{21}$$

Adding and subtracting these gives

$$[(\partial/\partial t) \pm (\rho a/\rho_o)(\partial/\partial h)]P \pm \rho a[(\partial/\partial t) \pm (\rho a/\rho_o)(\partial/\partial h)]u = 0$$

The original equations are now reduced to a directional derivative and

separate into ordinary differential equations along characteristic lines. Thus, along characteristic curves given by

$$dh/dt = \pm \rho a/\rho_o \tag{22}$$

the compatibility relations obtain:

$$dp \pm \rho a du = 0 \tag{23}$$

These, combined with Eq. (17)

$$(\partial S/\partial t)_h = 0$$

can be solved by stepwise integration to yield a solution to the flow for given initial and boundary conditions.

Where the wave propagates into a constant state (simple wave) entropy is the same throughout the flow and Eq. (23) can be integrated to give the Riemann integral:

$$u - u_o = \int dP/\rho a. \tag{24}$$

This relation is frequently used in the analysis of experimental data for rarefaction or continuous compression waves. By measuring the propagation speed of pressure or mass velocity increments, Eq. (23) can be integrated numerically to yield pressure-velocity and pressure-density relations. Note that this method is a special case of the general method outlined in Section III.A. For this case, as for steady flow, the two phase velocities, c_p and c_u, are equal since $P = P(u)$.

The characteristics method breaks down at shock fronts not necessarily because the shock becomes a discontinuity but because the assumption of an equilibrium equation of state is untenable.

D. Relaxing Elastic-Plastic Solids[38]

For elastic-plastic relaxing solids the assumption of particle-isentropic flow is retained, or, more accurately, the effect of entropy changes on the pressure-density relation is ignored. Nonequilibrium states are allowed, however, by assuming that the plastic strain-rates may be time-dependent, and that the stresses depend only on the elastic strains. The plastic strains are assumed incompressible.

The relation to be added to the conservation relations is:

$$(\partial P/\partial t) - a^2(\partial \rho/\partial t) = -F(P,\rho) \qquad (25)$$

where F is the plastic strain-rate multiplied by twice the shear modulus. The sound speed, a, is here the elastic longitudinal velocity, $a = \sqrt{(\lambda + 2\mu)/\rho}$. Combining this equation with Eqs. (7) and (8) in the same fashion as for isentropic flow in fluids yields the characteristic equations

$$c_+: \quad dP + \rho a du = -F dt, \quad \text{on } dh/dt = \rho a/\rho_0$$

$$c_-: \quad dP - \rho a du = -F dt, \quad \text{on } dh/dt = -\rho a/\rho_0$$

$$c_0: \quad dP - a^2 d\rho = -F dt, \quad \text{on } dh/dt = 0$$

These equations have been applied to the solution of plane wave propagation in quartzite, which exhibits pronounced time-dependent effects.[38] They have also been applied to infer the plastic strain-rate at the elastic yield point in iron from measurements of the decay in elastic amplitude.[40]

At the elastic shock front, when an elastic precursor wave exists, the jump conditions can be applied to relate P and u through the relation

$$P_1 = \rho_0 a u$$

Hence, on the leading c_+ characteristic,

$$dP/dt = -F/2$$

Measurements of the rate of change of peak stress thus yield a measure of the plastic strain rate at the elastic front. Since no time is assumed available for dislocation multiplication the plastic strain rate in turn determines the velocity of propagation of mobile dislocations.

In the general case, use of this theory to deduce constitutive relations from experiments requires that the constitutive relation be varied by postulating the function, $F(P,\rho)$, and comparing computed wave profiles with observations until agreement is achieved. A possible weakness is that "viscous" stresses are not permitted.

The relation between F and the phase velocities c_p and c_u is:

$$dP - a^2 d\rho = -Fdt \quad (\text{on } h = \text{const})$$

and

$$dP = (\rho_o{}^2/\rho^2)c_p c_u d\rho \quad (\text{on } h = \text{const})$$

Therefore,

$$-F = [1 - (a^2\rho^2/c_p c_u \rho_o{}^2)](\partial P/\partial t)_h$$

or if the speed of elastic longitudinal waves is expressed in Lagrangian coordinates:

$$a^* = a\rho/\rho_o$$

and

$$F = [(a^{*2}/c_p c_u) - 1](\partial P/\partial t)_h.$$

This relation can be used, within the context of the assumptions implied by Eq. (25), to determine the plastic strain rate associated with a measured pressure profile at any point of the profile. Note that vanishing of the plastic strain-rate implies that $c_p c_u = a^{*2}$ and that, in general, the product $c_p c_u$ is less than a^{*2}. To determine F from experiments, however, requires independent knowledge of a^*. It is not clear how this quantity can be unambiguously measured in wave experiments. However, acoustic measurements under hydrostatic pressure could provide the necessary data.

IV. EXPERIMENTAL RESULTS

A. Equations of State

At higher shock stresses, substantially exceeding the yield stress, the hydrostatic component of the stress tensor dominates and shock experiments effectively yield a hydrostatic equation of state. This is the Rankine-Hugoniot relation (Eq. (3)) mentioned earlier, with the x-component of stress, P, replaced by the mean stress, $\bar{P}$. At these pressures the elastic wave is either small enough to be neglected compared to the "plastic" or deformational shock, or may be overtaken by the plastic shock, i.e. a single shock may be stable. The shock rise-times are also usually very small so that the transition is effectively steady state whether or not the final state is a true equilibrium state. Hence, the R-H jump conditions can be applied to relate the shocked state to the initial state and the more elaborate analysis of Section III.A. is unnecessary.

A very large amount of data has been generated on equations of state, particularly of metals and rocks.[3,41-43] Where comparisons can be made with hydrostatic data the agreement is satisfactory,[44] and, in fact, shock data are used to calibrate static pressure apparatus in the higher pressure ranges.[45]

A principal uncertainty at the present time is the temperature of the shocked state, which can only be calculated with independent knowledge of, or assumptions about, the Gruneisen ratio and the specific heat.[3,41]

Attempts to measure temperature of the shocked state by means of the thermoelectric effect have thus far been unsuccessful.[46] Anomalously large signals have been observed whose physical origin is not understood. Some success has been achieved, however, in measuring free-surface temperatures.[47,48] These provide at least a consistency check on some of the assumptions employed in interpreting equation of state experiments.

By using porous samples R-H curves centered on different initial states (V_0,E_0) can be determined and the Gruneisen coefficient measured.[3,49] Thouvenin has questioned the assumption that equilibrium states can be achieved by this method,[50] but later work by Hofmann et al indicates that they are possible.[51]

B. Constitutive Relations

At shock stresses comparable to the yield stress, the effects of stress anisotropy and strain rate cannot be neglected. Not only does the elastic wave carry a significant fraction of the total stress, but the structure of the plastic shock and the rarefaction wave that relieves the shocked state are more complex. Figure 11 shows an example of the compressive portion of the wave shape in single crystal Lithium Fluoride. It would clearly be a coarse assumption to consider these waves as simply two discontinuities in stress separated by a constant region. Much more detailed analysis of the wave structure than simple application of the jump conditions is required.

Where strain-rate effects can be ignored, elastic-plastic theory can be applied to predict the differences between the one-dimensional constitutive relation and the hydrostatic equation of state.[11,52] This theory predicts the curves shown as Fig. 12. Above the yield point the difference between the normal stress in the direction of propagation and the hydrostatic pressure is just (2/3)Y, where Y is the yield stress in simple compression. Work-hardening can be incorporated. The release curve representing the states through which a rarefaction wave carries the material is also offset from the hydrostat by (2/3)Y once the yield stress in the reverse direction is attained.

Several attempts have been made to verify this model.[11,53] Measurements of the compressive state in aluminum indicate reasonably good agreement as indicated in Fig. 13. The rarefaction portion of the curve for the lower range of shock stresses shows poorer agreement, evidently because of Bauschinger effect.[36,54]

The Hugoniot elastic limit, indicated by P_o in Fig. 12, is frequently observed to be time-dependent and, as would be expected, is also dependent on the history of the specimen. Nevertheless, the values observed are approximately characteristic of the material and a useful tabulation of measurements to date has been given by Graham and Jones.[55]

At shock stresses of 100 kbar or more the difference between Hugoniot and hydrostat is difficult to resolve; moreover, good hydrostatic data do not exist. Measurements of the rate of decay of a shock pulse of finite width, however, permit inferences to be made about the yield stress and shear modulus under shock conditions.

The first experiments to observe shock decay were performed by Altshuler[56] and Curran[57] on aluminum. Curran's results indicated that shock decay is more rapid than would be predicted by the elastic-plastic model with constant yield stress. He postulated that yield stress increases with compression, attaining a value of 12 kbar at a relative volume, V/V_o, of 0.86. The initial yield stress was 0.5 kbar.

These results were verified, at least qualitatively, by Erkman.[58] He found similar behavior in copper and epoxy.

Recently, van Thiel and Kusubov have measured the shape of the rarefaction portion of an initially square pulse induced in aluminum by impact with a thin plate.[28] They used manganin gauges to interpolate between the peak pressure of the pulse and zero pressure. The impact pressure (130 kb) was higher than in Barker's similar experiments.[36] Their conclusion is that the yield stress is a peculiar function of pressure in the rarefaction wave and approaches values as high as 28 kbar, or nearly five times the static strength. (Fig. 14)

Their analysis is based on the assumption that the initial shocked state lies on the hydrostat rather than above it by (2/3)Y as predicted by elastic-plastic theory. Other experiments by these investigators, involving free-surface velocity measurements at an impact pressure of 313 kbar, indicate a yield stress of 14 kbar when analyzed according to conventional elastic-plastic theory.[59] The two sets of experimental results are compatible; the factor of two discrepancy is the result of different assumptions about the shocked state.

Similar experiments have been conducted in magnesium by Fuller and Price.[60] Their results are also compatible with the assumption that yield stress increases under pressure, attaining values perhaps two to five times the zero pressure value (1 kb) at a shock stress of 80 kb.

A limited amount of work comparing shock and hydrostatic compression has also been performed on covalent and ionic solids. The first experiments were those on quartz, which appeared to show that the stress difference, (2/3)Y, that might be expected between the R-H curve and the hydrostat above the yield point does not obtain.[61,62] The conclusion was that the material loses rigidity at the yield point and that, therefore, the yield mechanism is fundamentally different in those materials than in metals. Comparison of the shock data with more recent hydrostatic data,[63] however, does indicate an appreciable difference, so that the elastic-plastic model, modified to include stress relaxation, may be at least phenomenologically reasonable.* (Fig. 15) Similar results have also been obtained for Al_2O_3 in polycrystalline form.

Whether these latter results imply that brittle crystals such as quartz and Al_2O_3 can deform extensively by dislocation motion under shock conditions is not clear. If so, the dislocation mobilities must be substantially

*I am indebted to Dr. E. B. Royce for pointing this out. R. A. Graham points out, however, that the states above the elastic limit for different orientations of the quartz fall on the same curve. Moreover, there is a large reduction in electric polarization behind the second shock front. These observations are consistent with loss of rigidity above the elastic limit.

increased under shock. Recovered samples from experiments of this type are usually in the form of powder so that brittle fracture occurs somewhere in the shock and rarefaction process. Possibly fracture is the dominant yielding mechanism in the compression part of the wave, but intergranular friction maintains sufficient shear stress to give the stress differences observed. The shear stresses calculated for the elastic wave are very much higher than for metals and approach theoretical shear stresses for perfect crystals.[61,62]

It should be noted that other data still indicate a loss of rigidity above the yield point, notably in single crystal MgO[65] and Al_2O_3.[66]

Many materials, including metals and ionic and covalent crystals, exhibit stress relaxation. This is most easily observed in the decay of the elastic precursor wave with distance of travel from the impact surface, and in the structure of the wave between the elastic and plastic shock fronts. Stress relaxation, or strain-rate, effects are also important in the plastic shock front and, although the structure of this front can be resolved in many experiments at low stresses, only modest effort has thus far been made to correlate the shock structure with strain-rate models.

From the stress relaxation relations (Section III.D.) the plastic strain-rate at the elastic front can be determined from the rate of decay of the peak stress of the elastic wave. The relation is:

$$dP/dt = -F/2$$

where F is the plastic strain-rate multiplied by twice the shear modulus. This can be combined with the relation from dislocation theory:

$$\dot{\gamma} = (1/2)bNv$$

where $\dot{\gamma}$ is the plastic strain rate, b is the Burger's vector, N is the mobile dislocation density and v the velocity of dislocation motion.

Since the elastic front is very steep it is assumed that no time is available for multiplication of dislocations. Hence, $N = N_o$, the initial

dislocation density. If it is further assumed that, following Gilman, the dislocation velocities are given by,[40]

$$v = v^{\infty} \exp -D/\tau$$

where v^{∞} is the limiting dislocation velocity, D is a parameter called the drag stress, and τ is the shear stress, the equations above can be combined and integrated to give the peak elastic stress as a function of distance of travel and impact stress.[68] Comparison of the data then yields a set of compatible values for N_0 and D for a given impact stress.

The most detailed study of elastic precursor decay has been performed on Armco iron by Taylor.[40] His results are shown in Fig. 16. Reasonable values of N_0 and D do indeed give a good fit to these data, lending support to the theoretical model. Johnson, however, has recently pointed out that Taylor assumed that only one slip system of several possible systems was active in the (polycrystalline) iron.[67] If all systems are taken into account through an averaging process the necessary dislocation density is increased by a factor of about five. This density seems somewhat high compared to that obtained from independent measurements; consequently, the validity of the model is still somewhat tenuous. Kelly and Gillis point out that under the right conditions one might be able to discriminate between various dislocation models by experiments of this type.[68]

Precursor decay has also been studied in iron by Ivanov, et al,[69] in quartzite by Johnson,[39] and in aluminum by Barker, et al.[36]

Jones and Holland have studied the effect of grain size on the Hugoniot elastic limit in mild steel.[70] Although static tensile tests showed marked differences in the upper and lower yield point with varying grain size, no effect on the Hugoniot elastic limit was observed. They conclude that under the impact-loading conditions employed dislocations do not move far enough to encounter grain boundaries -- in contrast to the case of static yielding. The dynamic yield points, moreover, were two to three times those of the static experiments. They have also observed Bauschinger effects in pre-strained specimens.[71]

C. Porous Solids

There is considerable interest in shock propagation in porous solids, not only because equation of state data can be obtained over a wide range of densities and internal energies, as mentioned above, but also because porous solids possess excellent shock buffering characteristics. Hence, they can be used for the protection of structures from shock damage.

The collapse of pore space leads to large losses of internal energy as mechanical energy. In a steady state shock the internal energy is given by Eq. (3):

$$E - E_o = (P+P_o)(V_o-V)/2 \qquad (3)$$

The compressed specific volume is not highly sensitive to the energy; consequently, to a first approximation we can neglect the energy dependence of the P-V curve and visualize the energy loss as indicated in Fig. 17.

In the solid material, with initial volume V_s, a steady shock to pressure P_1 carries the material along the Rayleigh line joining P_1 and V_s. The triangular area under the Rayleigh line represents the internal energy of the shocked state. The portion of this internal energy recoverable as mechanical energy is approximately the area under the R-H curve. Hence the mechanical energy loss is the sliver-shaped area between the Rayleigh line and the associated R-H curve. Clearly, this area increases substantially with V_o as the porosity is increased.

The mechanisms for energy loss cannot be precisely stated because the solid is three-dimensional on the scale of the pore size. However, the principal mechanism is probably initially the conversion of directed kinetic energy in the propagation direction to acoustic energy propagating in random directions; various dissipative mechanisms then convert this energy to heat.

Thouvenin has proposed a one-dimensional model (plate-gap model) for a porous solid which allows no mechanism for energy losses.[50] Consequently,

he concludes that steady state shocks cannot exist, and predicts that a single R-H curve will be obtained for all initial densities. Hofmann, et al, have shown, however, that with an energy-dependent equation of state the plate-gap model approaches the continuum steady-state model with increasing time and propagation distance.[51] The question is therefore not which model is correct but under what conditions is each model correct. Little experimental work has yet been done to establish the conditions under which each model is valid.

The picture of the process shown in Fig. 17, although qualitatively correct, is very much simplified. The R-H curves are, of course, energy dependent so that each value of V_0 has its own associated P-V curve. At lower pressures the collapse of pore space may not be complete. Moreover, many porous solids exhibit a finite elastic yield stress so that a pressure pulse propagates as two or more wavefronts.

A more accurate, though still qualitative, P-V diagram is shown as Fig. 18. The elastic limit is indicated by P_e and the pressure at which the pore space has completely closed is indicated by P_c. The two R-H curves above P_c are separated because of greater shock heating of the initially porous material. Partial compaction occurs in the region between P_e and P_c, and following compaction the relief curve is substantially steeper than the compaction curve.

Linde and Schmidt[72] and Herrmann[73] have proposed phenomenological models for the P-V relation of porous solids, including the elastic yield point and the compaction region. Although they require experimentally determined parameters, these models appear to fit existing data reasonably well. The region of partial compaction is least well understood, especially the release curves from a compressed state.

The pressures at which pore collapse is complete depend on the material. Boade has reported that compaction is complete in porous copper at pressures of about 21 kbar.[74] In tungsten the compaction pressure is about 100 kbar[75] and in iron it is 26 kbar.[76] Aluminum and graphite evidently compact at lower pressures, of the order of a few kbar.[72]

Other models intermediate between the two mentioned have also been employed. The simple snow-plow model assumes zero elastic strength (P_e) and compaction pressure (P_c), and assumes further that the compacted material is perfectly rigid.[77] This model is very amenable to analysis and gives surprisingly accurate results for shock attenuation in highly distended materials. A modification which allows finite elastic strength but maintains the assumption of perfect rigidity of the compacted material has also been used for approximate analysis.

The elastic strength and the elastic wave speed are both substantially reduced by porosity. Butcher and Karnes have reported that the elastic precursor amplitude varies linearly with distention ratio from about 9.5 kbar in iron of zero porosity to 1.5 kbar at a distention ratio (i.e. ratio of initial density of solid to initial density of porous solid) of 1.63.[78] The elastic wave velocity also varies linearly from 6.0 km/sec at zero porosity to 1.15 km/sec at a distention ratio of 2.37. These results seem to be typical for most porous solids investigated to date.

A third wave has been observed in copper by Boade.[74] The first travels with acoustic velocity with an amplitude of a few tenths of a kbar; the second travels with a velocity of about half the acoustic velocity and an amplitude of 1.35 kbar. These waves are followed by a third that carries the material to the peak pressure. The origin of the second wave is unclear; it may be related to a distinct stage of the compaction process.

The shock profiles observed in porous iron, graphite, and aluminum are not steady but continue to spread in the specimen thicknesses employed in the experiments.[72,76] The physical mechanisms for stress relaxation are not established; however, it is possible that the experiments are observing the transition from the plate-gap model to the continuum steady state model.

D. Plastics

Only a limited amount of information is available for plastics in the stress range at which one expects nonhydrostatic effects to be appreciable. Poly methyl methacrylate (Plexiglas), however, has been studied by several investigators and it is reasonable to suppose that its behavior is typical of many polymers.[79-81] An excellent discussion of its high pressure behavior has been given by Deal.[82]

There are two distinctive features of the shock response of plexiglas that are in marked contrast to the behavior of metals or of brittle solids. An elastic precursor wave has never been observed even at low impact stresses, and evidently one does not exist.[79-81] The observed shock velocities, moreover, extrapolate to the longitudinal sound speed at zero stress. It is not reasonable to suppose that the shear stresses increase indefinitely with shock stress, although Ainbinder, et al, have observed an increase by nearly a factor of two in yield stress under confining pressures of about 2 kbar.[83] It may be that yielding occurs over a wide stress range so that a cusp in the P-V curve (Fig. 2) never appears. Measurement of release curves or comparison of shock data with hydrostatic data would provide valuable information about the shear stresses. Experiments on epoxy at stresses as low as 3.2 kbar also show no indication of an elastic wave.[84] That epoxy cannot be treated as a fluid is indicated by Erkman's data on shock decay.[58] (Fig. 19)

Plexiglas also exhibits pronounced relaxation of the shocked state with propagation distance in experiments in which rarefaction waves from boundaries cannot influence the shock front.[85] Thus, it is a highly rate-sensitive material.

Kolsky has devised a constitutive relation for polymers that successfully predicts the pulse shapes in plexiglas and polyethylene in the low stress range in rod or spherical wave geometry.[86] It is based on a viscoelastic model and employs an empirically determined value, assumed independent of frequency, for the phase angle between the stress and strain amplitudes in a sinusoidal wave. It would seem fruitful to attempt to apply his analysis to plane waves as well, and to try to extend it to include nonlinear stress-strain behavior.

V. CONCLUSIONS

The subject of one-dimensional-strain constitutive relations applicable to shock propagation, with the possible exception of high pressure equation of state measurements, is clearly in its infancy. As experimental techniques become more refined the concepts and assumptions of gas dynamics, such as discontinuous shock fronts and equilibrium, isentropic rarefactions, which formed the early foundation for the subject appear to lose pertinency. Certainly, the assumption of isotropic stress even at stresses very much in excess of the yield stress has been found to be questionable. Stress relaxation effects also seem to be very common.

Because of the often severe distortion of the shock structure by reflections at interfaces, the techniques which seem to hold the best promise for significant advances in understanding are those that can be imbedded in the material, such as piezoresistive gauges, electromagnetic velocity gauges, and, for transparent substances, optical methods. Quartz and sapphire gauges, of course, should be added to this list where the shock impedance of the sample is closely matched. These, combined with a general analytical treatment such as that outlined in Section III, should provide a sounder base of experimental information than currently exists.

The elastic-plastic model has been demonstrated to give reasonable predictions for metals when rate effects are not large and at stresses only moderately exceeding the yield stress. Rate effects are the subject of much current research and it may be expected that progress will be made in understanding not only such phenomena as the decay of elastic precursor waves, but, perhaps more importantly, the physics of the plastic shock transition itself. The behavior of the yield stress at higher pressures is clearly not well understood; whether or not it increases substantially with pressure and to what extent the Bauschinger effect is important are still controversial topics.

Brittle solids are even less well understood and one cannot predict with confidence whether for a given material substantial shear stresses can exist behind the "plastic" shock front, nor what the release paths from a

shocked state may be. Many of these solids are further complicated by phase transformations.

Plastics appear to comprise another distinct class of materials for which a model for the constitutive relation under shock needs formulation. Much more experimentation is required before theory can fairly begin on this problem, although the success of Kolsky's model at low stresses is encouraging.

Porous solids form still another class in which much work is currently underway. The nature of the compaction process is only beginning to be understood and is crucial to predictions of shock propagation.

TABLE I

Stresses Produced by Impact at 1.5 mm/μs. (kbar)

Projectile	Target				
	Al	Fe	Pb	W	Lucite
Al	130	175	175	235	30
Fe	175	280	275	390	70
Pb	175	275	270	385	70
W	235	390	385	640	75
Lucite	30	70	70	75	30

ACKNOWLEDGEMENT

This work was supported by the Air Force Office of Scientific Research (ARPA), Office of Aerospace Research, United States Air Force, under Contract No. F44620-67-C-0087. I wish to thank Dr. G. E. Duvall for reading the manuscript and for thoughtful suggestions.

REFERENCES

1) J. F. Bell, 'The Dynamic Plasticity of Metals at High Strain Rates: An Experimental Generalization," in BEHAVIOR OF MATERIALS UNDER DYNAMIC LOADING, Am. Soc. Mech. Engr., 19 (1965).

2) G. E. Duvall and G. R. Fowles, "Shock Waves," in HIGH PRESSURE PHYSICS AND CHEMISTRY, R. S. Bradley, Ed., Vol. 2, Academic Press (1963).

3) L. V. Al'tshuler, "Use of Shock Waves in High Pressure Research," Soviet Physics-Uspekhi 8, 52 (1965).

4) S. D. Hamman, "Effects of Intense Shock Waves," in ADVANCES IN HIGH PRESSURE RESEARCH, R. S. Bradley, Ed., Academic Press (1966).

5) I. C. Skidmore, "An Introduction to Shock Waves," Applied Materials Research, 131 (July 1965).

6) G. E. Duvall, "Shock Waves in the Study of Solids," Appl. Mech. Rev. 15, 849 (1962).

7) C. H. Karnes, "The Plate Impact Configuration for Determining Mechanical Properties of Materials at High Strain Rates," Symposium on the Mechanical Behavior of Materials under Dynamic Loads, U.S. Army Research Office, Durham, N. C. (1967).

8) R. Courant and K. Friedrichs, SUPERSONIC FLOW AND SHOCK WAVES, Interscience (1948).

9) Wm. Band, "Studies in the Theory of Shock Propagation in Solids," J. Geophys. Res. 65, 695 (1960).

10) D. R. Bland, "On Shock Structure in a Solid," J. Inst. Maths Applics. 1, 56 (1965).

11) G. R. Fowles, "Shock Wave Compression of Hardened and Annealed 2024 Aluminum," J. Appl. Phys. 32, 1475 (1961).

12) S. Thunborg, Jr., G. E. Ingram and R. A. Graham, "Compressed Gas Gun for Controlled Planar Impacts over a Wide Velocity Range," Rev. Sci. Instr. 35, 11 (1964).

13) L. M. Barker and R. E. Hollenbach, "System for Measuring the Dynamic Properties of Materials," Rev. Sci. Instr. 35, 742 (1964).

14) G. R. Fowles, et al, "Gas Gun for Impact Studies," Bull. Am. Phys. Soc. II, 13, #12, 1680 (Dec. 1968). (Article to be published.)

15) A. E. Seigel, "The Theory of High Speed Guns," Agardograph 91, U.S. Naval Ordnance Laboratory, Silver Spring, Maryland (1965).

16) L. M. Barker and R. E. Hollenbach, "Interferometer Technique for Measuring the Dynamic Mechanical Properties of Materials," Rev. Sci. Instr. 36, 1617 (1965).

17) W. M. Isbell, F. H. Shipman and A. H. Jones, "Use of a Light Gas Gun in Studying Material Behavior at Megabar Pressures," in BEHAVIOUR OF DENSE MEDIA UNDER HIGH DYNAMIC PRESSURES, Symposium H.D.P., p. 179, Gordon and Breach, N. Y. (1968).

18) A. H. Jones, W. M. Isbell and C. J. Maiden, "Measurement of the Very-High-Pressure Properties of Materials using a Light Gas Gun," J. Appl. Phys. 37, 3493 (1966).

19) J. Shea, Private Communication (1969).

20) J. C. Bushnell and D. J. McCloskey, "Thermoelastic Stress Production in Solids," J. Appl. Phys. 39, 5541 (1968).

21) R. A. Graham, F. W. Neilson and W. B. Benedick, "Piezoelectric Current from Shock-Loaded Quartz -- A Submicrosecond Stress Gauge," J. Appl. Phys. 36, 1775 (1965).

22) D. G. Doran, "Measurement of Shock Pressures in Solids," in HIGH PRESSURE MEASUREMENT, Giardini and Lloyd, Eds., Butterworths (1963).

23) W. E. Deal, "Dynamic High Pressure Techniques," in MODERN VERY HIGH PRESSURE TECHNIQUES, R. H. Wentorf, Ed., 200, Butterworth, London (1962).

24) P. W. Bridgman, Proc. Amer. Acad. Arts Sci. 47, 321 (1911).

25) D. Bernstein and D. D. Keough, "Piezoresistivity of Manganin," J. Appl. Phys. 35, 1471 (1964).

26) P. J. A. Fuller and J. H. Price, "Dynamic Pressure Measurements to 300 Kilobars with a Resistance Transducer," Brit. J. Appl. Phys. 15, 751 (1964).

27) D. D. Keough and R. F. Williams, "Piezoresistive Transducer for Shock Wave Studies," AFWL-TR-67-81, Air Force Weapons Laboratory, Kirtland AFB, N. Mex. (1967).

28) M. van Thiel and A. Kusubov, "Effect of 2024 Aluminum Alloy Strength on High Pressure Shock Measurements," Proc. of "Symposium on Accurate Characterization of High Pressure Environment," National Bureau of Standards, Gaithersburg, Md. (1968).

29) E. O. Williams, "An Etched Manganin Gage System for Shock Pressure Measurement in a High Noise Environment," SCL-DC-67-92, Sandia Corporation, Livermore, California (1967).

30) R. Williams and D. D. Keough, "Piezoresistive Response of Thin Films of Calcium and Lithium to Dynamic Loading," Bull. Am. Phys. Soc., Series II, 12, No. 8, 1127 (1967).

31) D. Bernstein, C. Godfrey, A. Klein and W. Shimmin, "Research on Manganin Pressure Transducers," in BEHAVIOUR OF DENSE MEDIA UNDER HIGH DYNAMIC PRESSURES, Symposium H.D.P., 461, Gordon and Breach, N. Y. (1968).

32) A. N. Dremin and G. A. Adadurov, "The Behavior of Glass under Dynamic Loading," Soviet Physics-Solid State 6, 1379 (1964).

33) D. L. Ainsworth and B. R. Sullivan, "Shock Response of Rock at Pressures below 30 Kilobars," Tech. Report No. 6-802, U.S. Army Engineer Waterways Experiment Station, Vicksburg, Miss. (1967).

34) G. R. Danker, Private Communication.

35) R. Graham and G. E. Ingram, "A Shock Wave Stress Gage Utilizing the Capacitance Charge of a Solid Dielectric Disc," in BEHAVIOUR OF DENSE MEDIA UNDER HIGH DYNAMIC PRESSURES, Symposium H.D.P., 469, Gordon and Breach, N. Y. (1968).

36) L. M. Barker, "Fine Structure of Compressive and Release Wave Shapes in Aluminum Measured by the Velocity Interferometer Technique," in BEHAVIOUR OF DENSE MEDIA UNDER HIGH DYNAMIC PRESSURES, Symposium H.D.P., 483, Gordon and Breach, New York (1968).

37) Roger Williams, Private Communication (1969).

38) G. E. Duvall, "Propagation of Plane Shock Waves in a Stress-Relaxing Medium," in STRESS WAVES IN ANELASTIC SOLIDS, Kolsky and Prager, Eds., Springer-Verlag, Berlin (1963).

39) J. N. Johnson, "Shock Waves in Stress-Relaxing Solids," Ph.D. Thesis, Washington State University (1966).

40) J. W. Taylor, "Dislocation Dynamics and Dynamic Yielding," J. Appl. Phys. 36, 3146 (1965).

41) M. H. Rice, R. G. McQueen and J. M. Walsh, "Compression of Solids by Strong Shock Waves," in SOLID STATE PHYSICS, Vol. 6, Seitz and Turnbull, Eds., Academic Press (1958).

42) R. G. McQueen and S. P. Marsh, "Equation of State of Nineteen Metallic Elements from Shock Wave Measurements to 2 Mbar," J. Appl. Phys. 31, 1253 (1960).

43) R. G. McQueen, S. P. Marsh and J. N. Fritz, "Hugoniot Equation of State of Twelve Rocks," J. Geophys. Res. 72, No. 20, 4999 (1967).

44) D. E. Munson and L. M. Barker, "Dynamically Determined Pressure-Volume Relationships for Aluminum, Copper and Lead," J. Appl. Phys. 37, 1652 (1966).

45) E. A. Perez-Albuerne, K. F. Forsgren and H. G. Drickamer, "Apparatus for X-Ray Measurements at Very High Pressure," Rev. Sci. Instr. 35, 29 (1964).

46) J. Crosnier, J. Jacquesson and A. Migault, "Anomalous Thermoelectric Effect in the Shock Regime and Application to a Shock Pressure Transducer," in PROCEEDINGS OF FOURTH SIMPOSIUM (INTERNATIONAL) ON DETONATION, ACR-126, Office of Naval Research - Department of the Navy, Washington D.C. (1965).

47) J. W. Taylor, "Residual Temperatures of Shocked Copper," J. Appl. Phys. 34, 2727 (1963).

48) P. J. King, D. F. Cotgrove and P. M. B. Slate, "Infrared Method of Estimating the Residual Temperatures of Shocked Metal Plates," in BEHAVIOUR OF DENSE MEDIA UNDER HIGH DYNAMIC PRESSURES, Symposium H.D.P., Gordon and Breach, New York (1968).

49) G. D. Anderson and A. L. Fahrenbruch, "Equation of State of Solids, II. Aluminum and Teflon," Tech. Report No. AFWL-TR-67-43, Air Force Weapons Laboratory, Kirtland AFB, New Mexico (1967).

50) J. Thouvenin, "Effect of a Shock Wave on a Porous Solid," in

PROCEEDINGS OF FOURTH SYMPOSIUM (INTERNATIONAL) ON DETONATION, ACR-126, 258, Office of Naval Research - Dept. of the Navy, Washington, D.C. (1965).

51) R. Hofmann, D. J. Andrews and D. E. Maxwell, "Computed Shock Response of Porous Aluminum," J. Appl. Phys. 39, 4555 (1968).

52) L. W. Morland, "The Propagation of Plane Irrotational Waves Through an Elastoplastic Medium," Phil. Trans. Roy. Soc. A251, 341 (1959).

53) C. D. Lundergan and W. Herrmann, J. Appl. Phys. 34, 2046 (1963).

54) L. M. Barker, C. D. Lundergan and W. Herrmann, "Dynamic Response of Aluminum," J. Appl. Phys. 35, 1203 (1964).

55) R. A. Graham and O. E. Jones, "A Summary of Hugoniot Elastic Limit Measurements," SC-R-68-1857, Sandia Corporation, Albuquerque (1968).

56) L. V. Al'tshuler, et al, "The Isentropic Compressibility of Aluminum, Copper, Lead, and Iron at High Pressures," Soviet Physics-JETP 11, 766 (1960).

57) D. R. Curran, "Non-Hydrodynamic Attenuation of Shock Waves in Aluminum," J. Appl. Phys. 34, 2677 (1963).

58) J. O. Erkman, "Elastoplastic Effects in the Attenuation of Shock Waves," in PROCEEDINGS OF FOURTH SYMPOSIUM (INTERNATIONAL) ON DETONATION, ACR-126, 277, Office of Naval Research, Dept. of the Navy, Washington, D.C. (1965).

59) A. S. Kusubov and M. van Thiel, "Dynamic Yield Strength of 2024-T4 Aluminum at 313 kbar," J. Appl. Phys. 40, 893 (1969).

60) P. J. A. Fuller and J. H. Price, "The Elasto-Plastic Release Behaviour of Magnesium at 80 Kbar," in PROCEEDINGS OF FOURTH SYMPOSIUM (INTERNATIONAL) ON DETONATION, ACR-126, 290, Office of Naval Research, Department of the Navy, Washington, D.C. (1965).

61) J. Wackerle, "Shock Compression of Quartz," J. Appl. Phys. 33, 922 (1962).

62) R. Fowles, "Dynamic Compression of Quartz," J. Geophys. Res. 72, 5729 (1967).

63) D. B. McWhan, "Linear Compression of α-quartz to 150 Kbar," J. Appl. Phys. 38, 347 (1967).

64) T. J. Ahrens, W. H. Gust and E. B. Royce, "Material Strength Effect in the Shock Compression of Alumina," J. Appl. Phys. 39 (1968).

65) T. J. Ahrens, "High Pressure Electrical Behavior and Equation of State of Magnesium Oxide from Shock Wave Experiments," J. Appl. Phys. 37, 2532 (1966).

66) W. P. Brooks and R. A. Graham, Bull. Am. Phys. Soc. 11, 414 (1966).

67) J. N. Johnson, "A Rate-Dependent Constitutive Relation for Polycrystalline Metals," Preprint, Sandia Corporation, Albuquerque, N. Mex. (1969).

68) J. M. Kelly and P. P. Gillis, "Dislocation Dynamics and Precursor Attenuation," J. Appl. Phys. 38, 4044 (1967).

69) A. G. Ivanov, S. A. Novikov and V. A. Sinitsyn, "Investigation of Elastic-Plastic Waves in Explosively Loaded Iron and Steel," Soviet Physics-Solid State 5, 196 (1963).

70) O. E. Jones and J. R. Holland, "Effects of Grain Size on Dynamic Yielding in Explosively Loaded Mild Steel," Acta Met. 16, 1037 (1968).

71) O. E. Jones and J. R. Holland, J. Appl. Phys. 35, 1771 (1964).

72) R. K. Linde and D. N. Schmidt, "Shock Propagation in Nonreactive Porous Solids," J. Appl. Phys. 37, 3259 (1966).

73) W. Herrmann, "Equation of State of Crushable Distended Materials," SC-RR-66-2678, Sandia Corporation, Albuquerque, New Mexico (1968).

74) R. R. Boade, "Compression of Porous Copper by Shock Waves," J. Appl. Phys. 39, 5693 (1968).

75) R. R. Boade, "Shock Loading of Porous Tungsten," SC-RR-66-290, Sandia Corporation, Albuquerque, New Mexico (1966).

76) P. C. Lysne and W. J. Halpin, "Shock Compression of Porous Iron in the Region of Incomplete Compaction," J. Appl. Phys. 39, 5488 (1968).

77) J. R. Rempel and D. N. Schmidt, "Shock Behavior of Some Non-Reacting Porous Solids," in PROCEEDINGS OF FOURTH SYMPOSIUM (INTERNATIONAL) ON DETONATION, ACR-126, Office of Naval Research, Department of the Navy, Washington, D.C. (1965).

78) B. M. Butcher and C. H. Karnes, "Dynamic Compaction of Porous Iron," SC-RR-67-3040, Sandia Corporation, Albuquerque, N. Mex. (1968).

79) D. N. Schmidt and M. W. Evans, "Shock Wave Compression of Plexiglas in the 2.5 to 20 Kilobar Region," Nature 206, 1348 (1965).

80) T. P. Liddiard, Jr., "The Compression of Polymethyl Methacrylate by Low Amplitude Shock Waves," in PROCEEDINGS OF FOURTH SYMPOSIUM (INTERNATIONAL) ON DETONATION, ACR-126, 214, Office of Naval Research, Department of the Navy, Washington, D.C. (1965).

81) W. J. Halpin and R. A. Graham, "Shock Wave Compression of Plexiglas from 3 to 20 Kilobars," in PROCEEDINGS OF FOURTH SYMPOSIUM (INTERNATIONAL) ON DETONATION, ACR-126, 222, Office of Naval Research, Department of the Navy, Washington, D.C. (1965).

82) W. E. Deal, "Shock Wave Research on Inert Solids," in PROCEEDINGS OF FOURTH SYMPOSIUM (INTERNATIONAL) ON DETONATION, ACR-126, 321, Office of Naval Research, Department of the Navy, Washington, D.C. (1965).

83) S. B. Ainbinder, M. G. Lake and I. Yu. Maiors, "Effect of Hydrostatic Pressure on the Resistance to Deformation and the Strength of Polymer Materials," Soviet Physics-Doklady 9, 1127 (1965).

84) T. R. Guess, "Some Dynamic Mechanical Properties of an Epoxy," SC-DR-68-343, Sandia Corporation, Albuquerque, New Mexico (1968).

85) D. V. Keller, "Behavior of Short Duration Shocks in Plexiglas," in BEHAVIOUR OF DENSE MEDIA UNDER HIGH DYNAMIC PRESSURES, Symposium H.D.P., 453, Gordon and Breach, New York (1968).

86) H. Kolsky, "The Propagation of Mechanical Pulses in Anelastic Solids," in BEHAVIOR OF MATERIALS UNDER DYNAMIC LOADING, Am. Soc. Mech. Engrs., New York.

87) J. Asay, Private Communication (1969).

88) P. W. Bridgman, "The Compression of 39 Substances to 100,000 kg/cm^2," COLLECTED EXPERIMENTAL PAPERS, Vol. 6, pp. 160-3819, Harvard University Press, Boston, Mass. (1947).

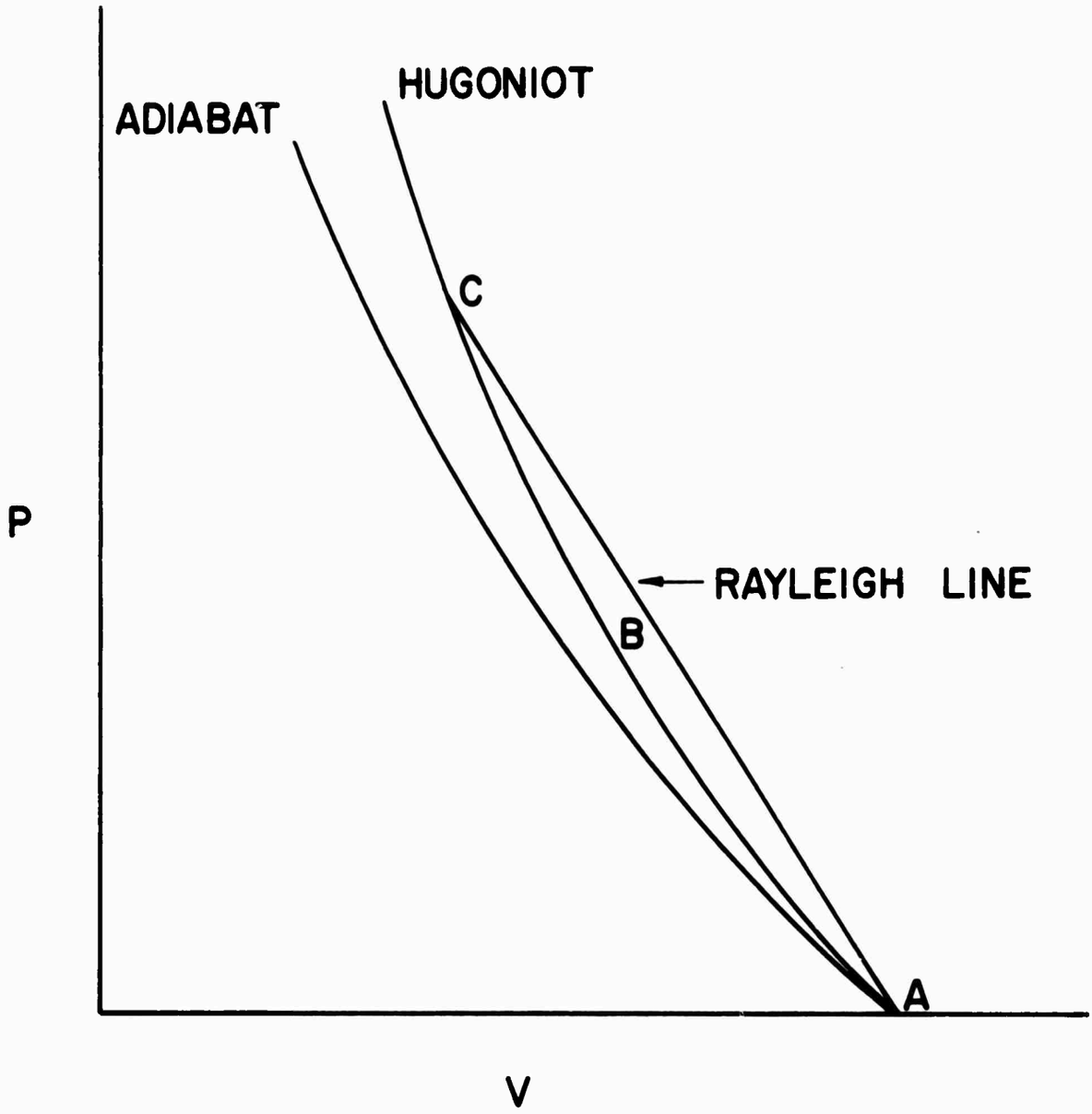

Figure 1. Pressure-Volume Curves for a Simple Fluid. The Hugoniot curve is the locus of equilibrium end states attainable through a series of steady shock transitions. The straight line is the Rayleigh line for a shocked state, "C".

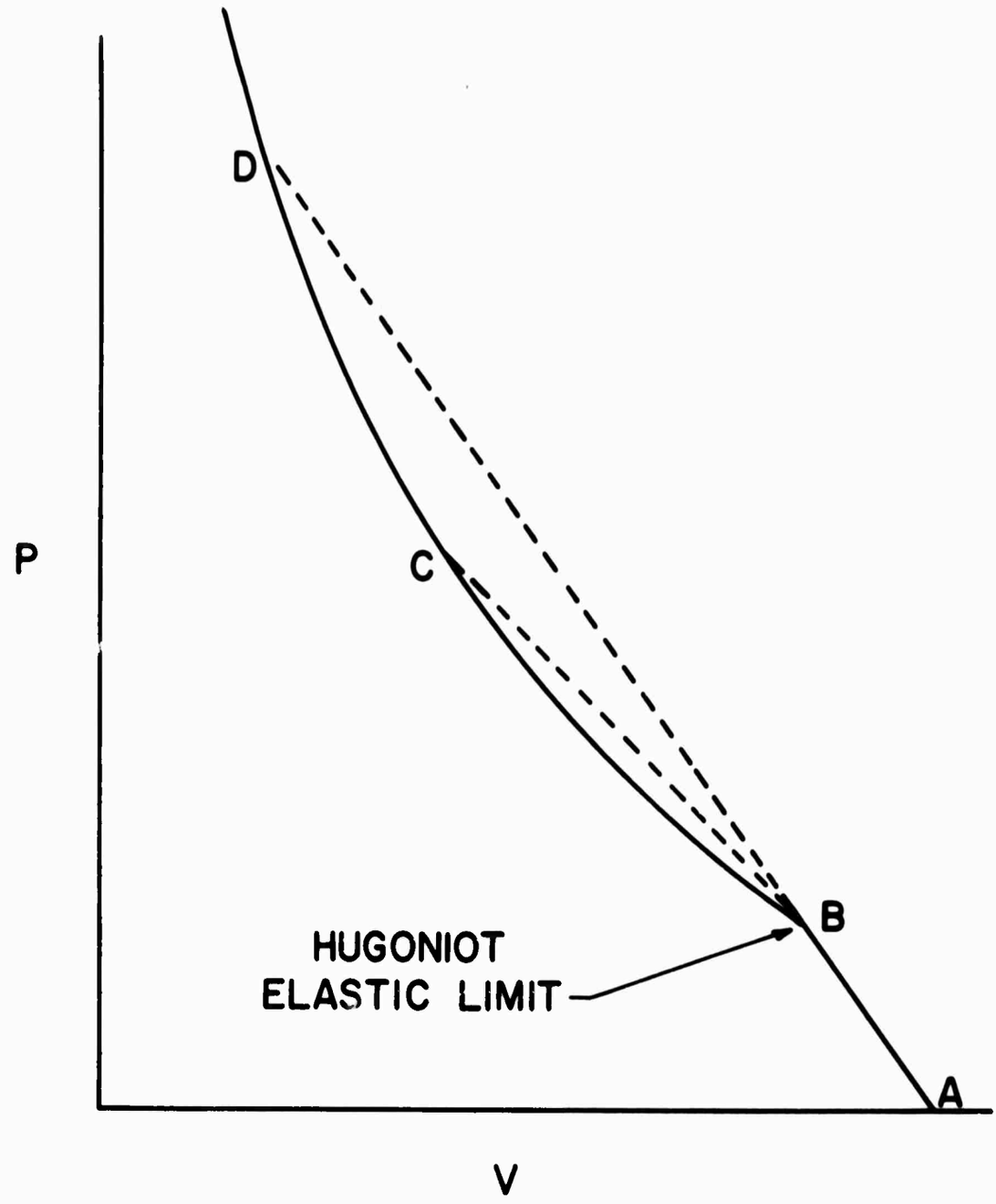

Figure 2. Hugoniot Curve for a Solid Showing a Cusp at the Elastic Limit. A single shock front is stable at stresses less than "B" or greater than "D". Intermediate shock amplitudes propagate as two wavefronts.

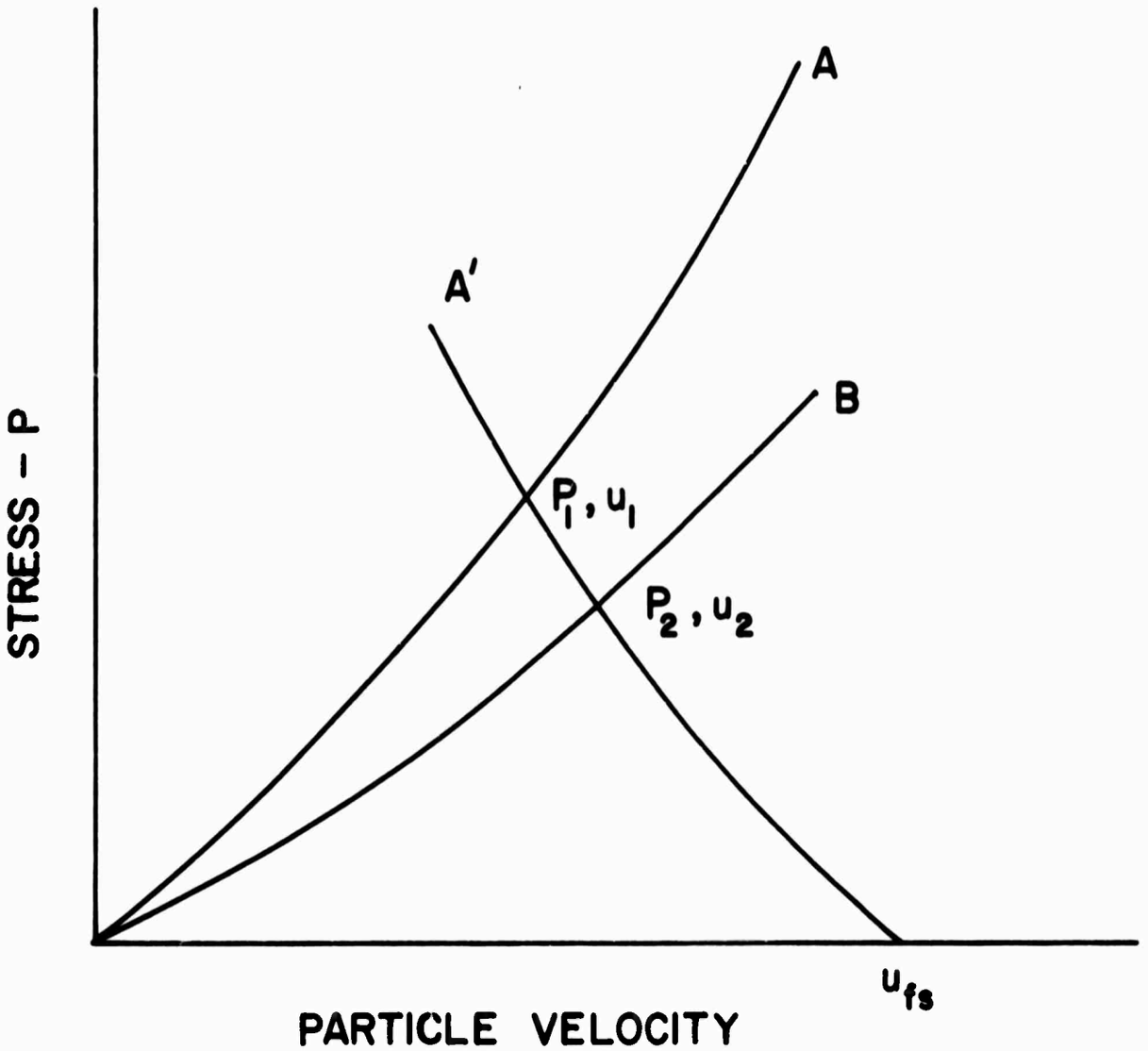

Figure 3. Stress-Velocity Curves. A shock in Material "A" with state (P_1,u_1) reflects at an interface with material "B" to produce the common state, (P_2,u_2). The curves A' and A are the same when entropy changes can be neglected.

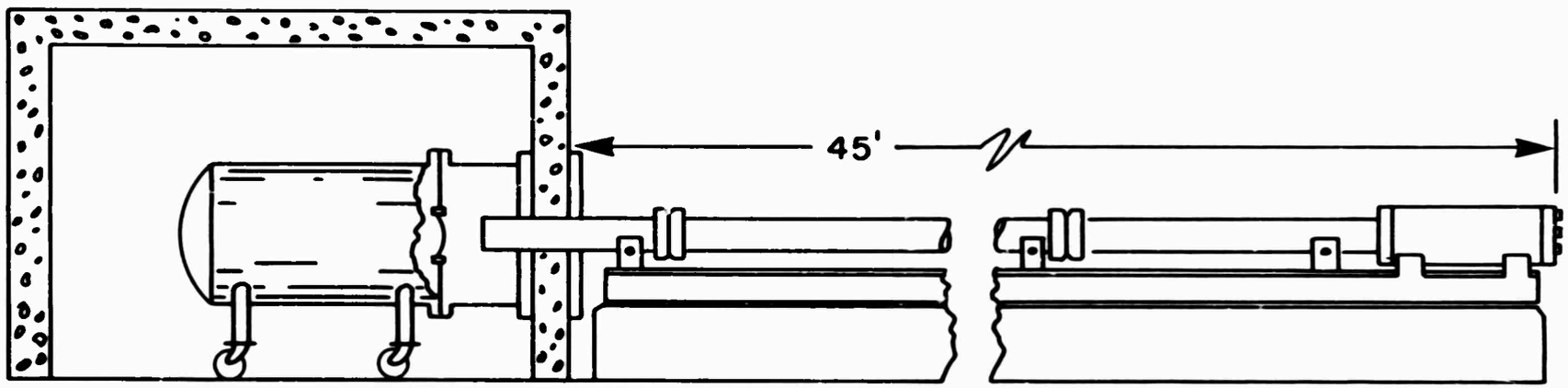

Figure 4. Sketch of WSU Gas Gun.[14] The entire gun slides freely to absorb recoil. The target is mounted rigidly to the wall of the muzzle room. The catcher tank prevents damage to the muzzle room and substantially reduces noise.

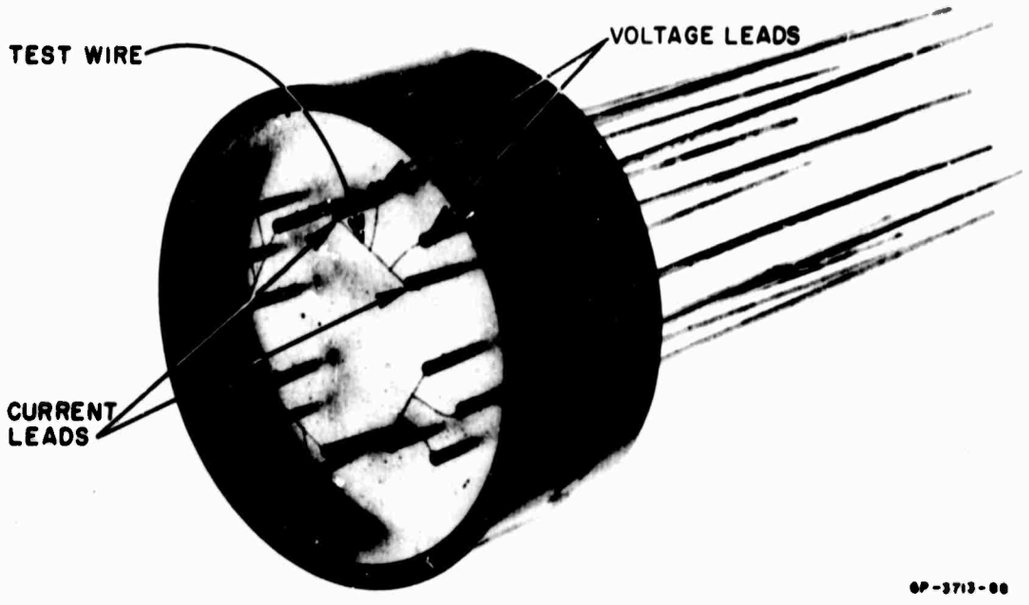

Figure 5. Manganin Pressure Transducer. Four pi-shaped manganin wires are shown imbedded in epoxy. The change in voltage is monitored as the shock passes over the wires. Current is held constant. (After Keough[27])

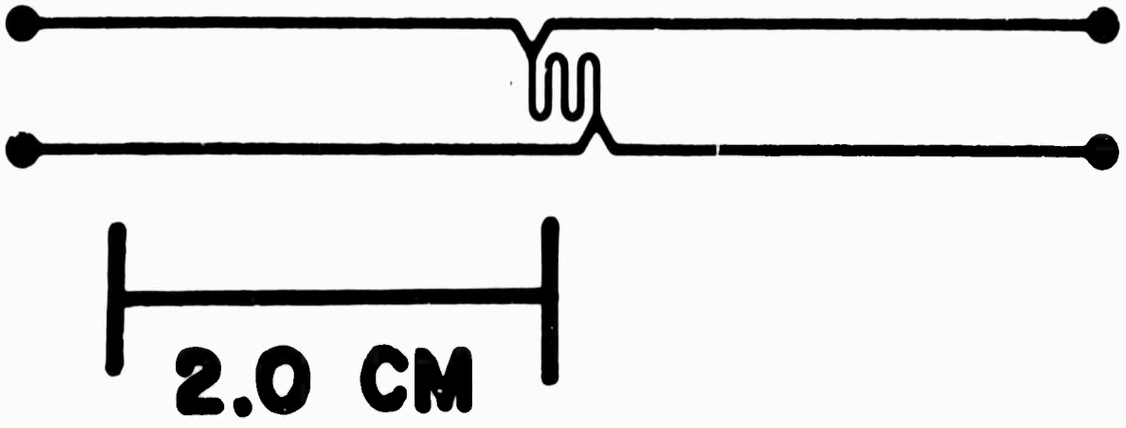

Figure 6. Manganin Grid for use as In-Material Gauge. Thickness is 0.75 x 10^{-3} in. Resistance of active element is about 1.5 ohms.

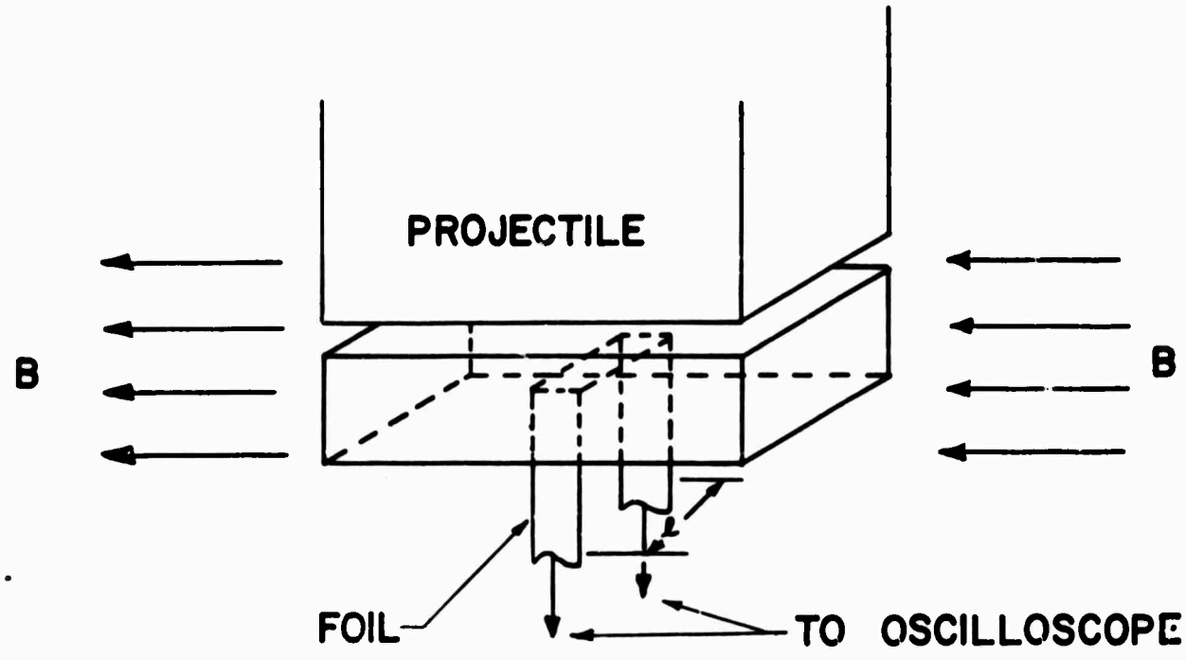

Figure 7. Schematic of Electromagnetic Velocity Technique. Motion of foil imbedded in insulator is monitored by observing EMF developed.

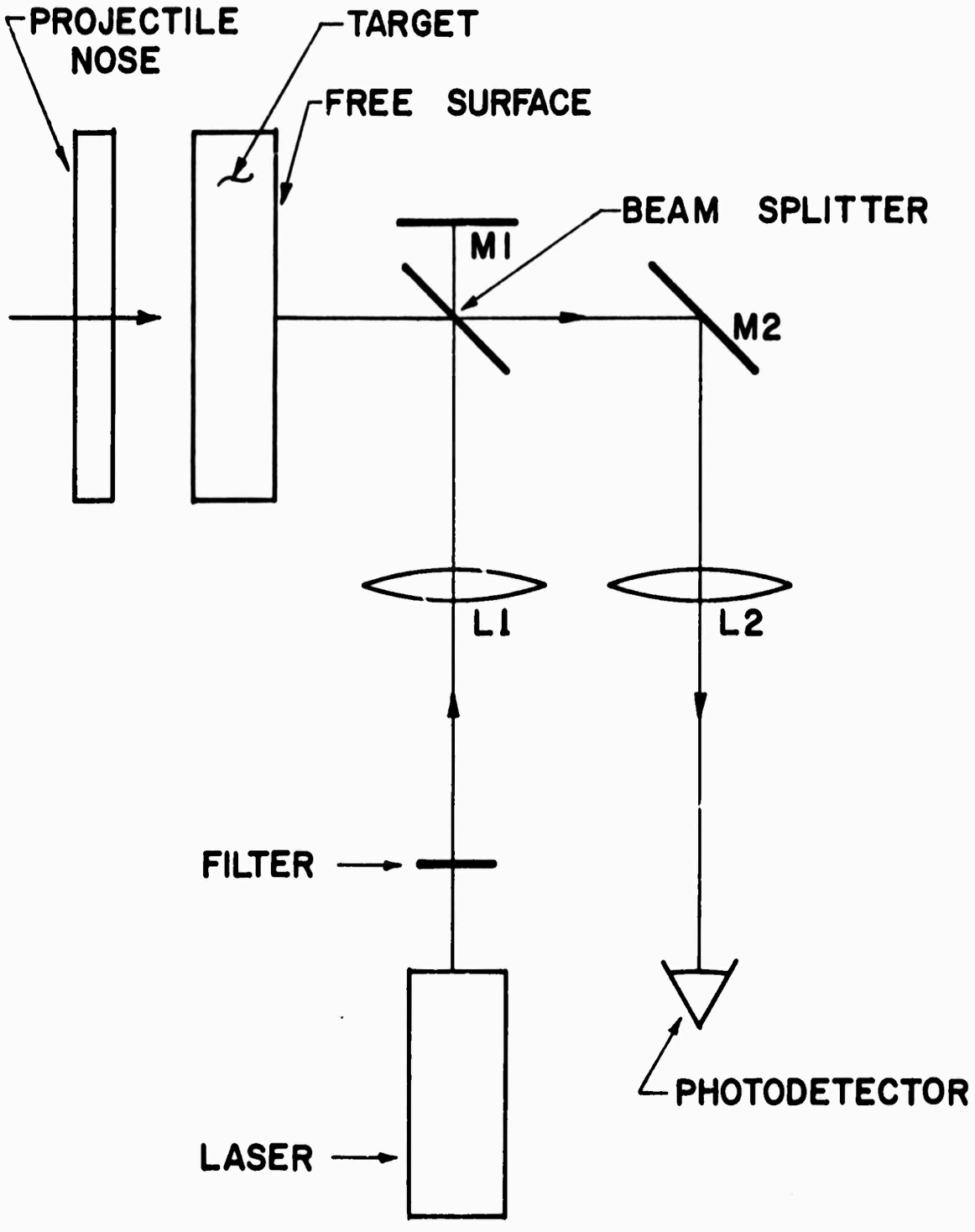

Figure 8. Laser Interferometer. Fringes developed by interference of beams reflected from moving and stationery mirrors record displacement of target free-surface. (After Barker[16])

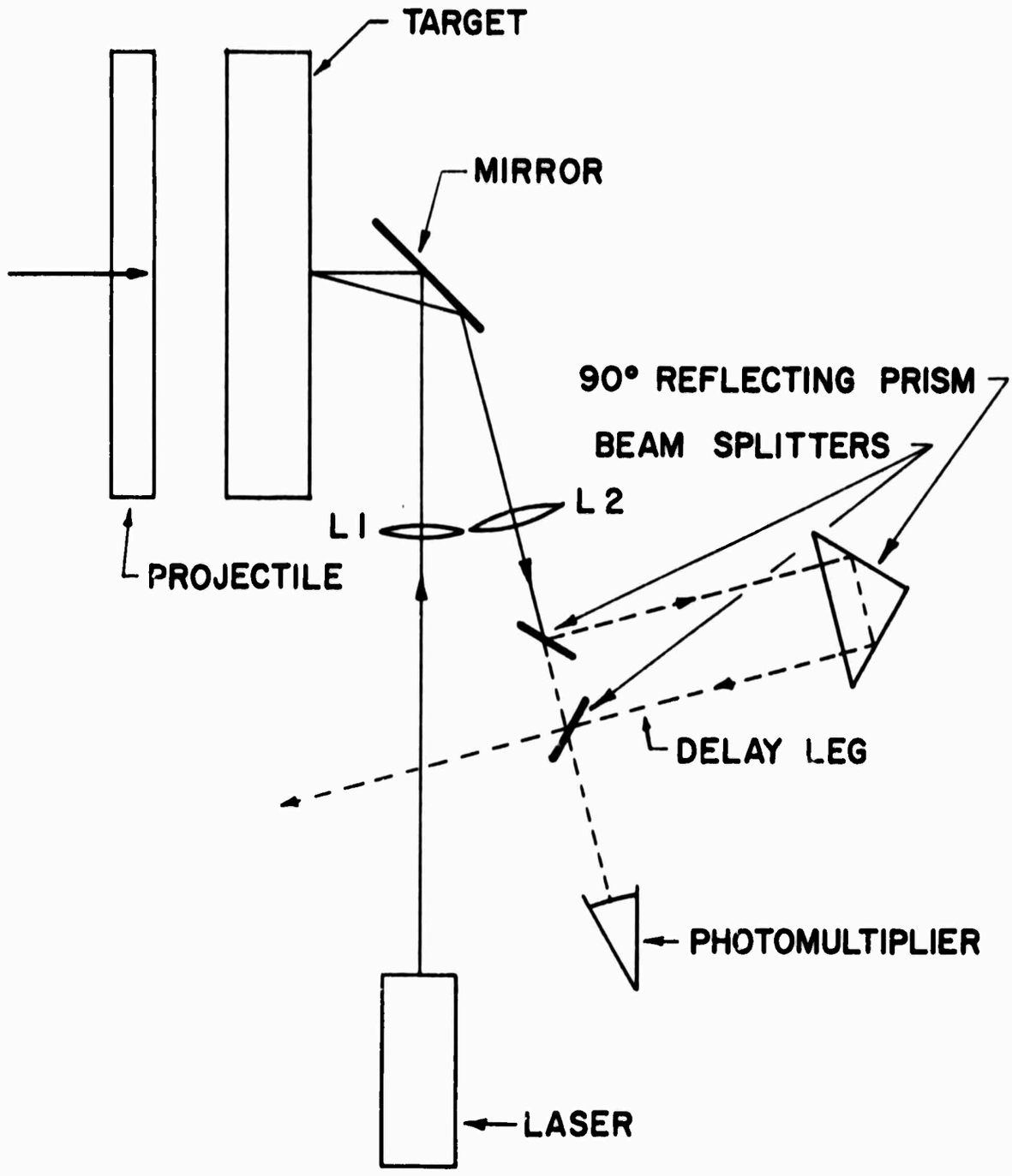

Figure 9. Velocity Interferometer. Fringes are developed by interference of reflected beam with that reflected from same surface earlier in time. Fringe counting rate is proportional to acceleration of surface. (After Barker[36])

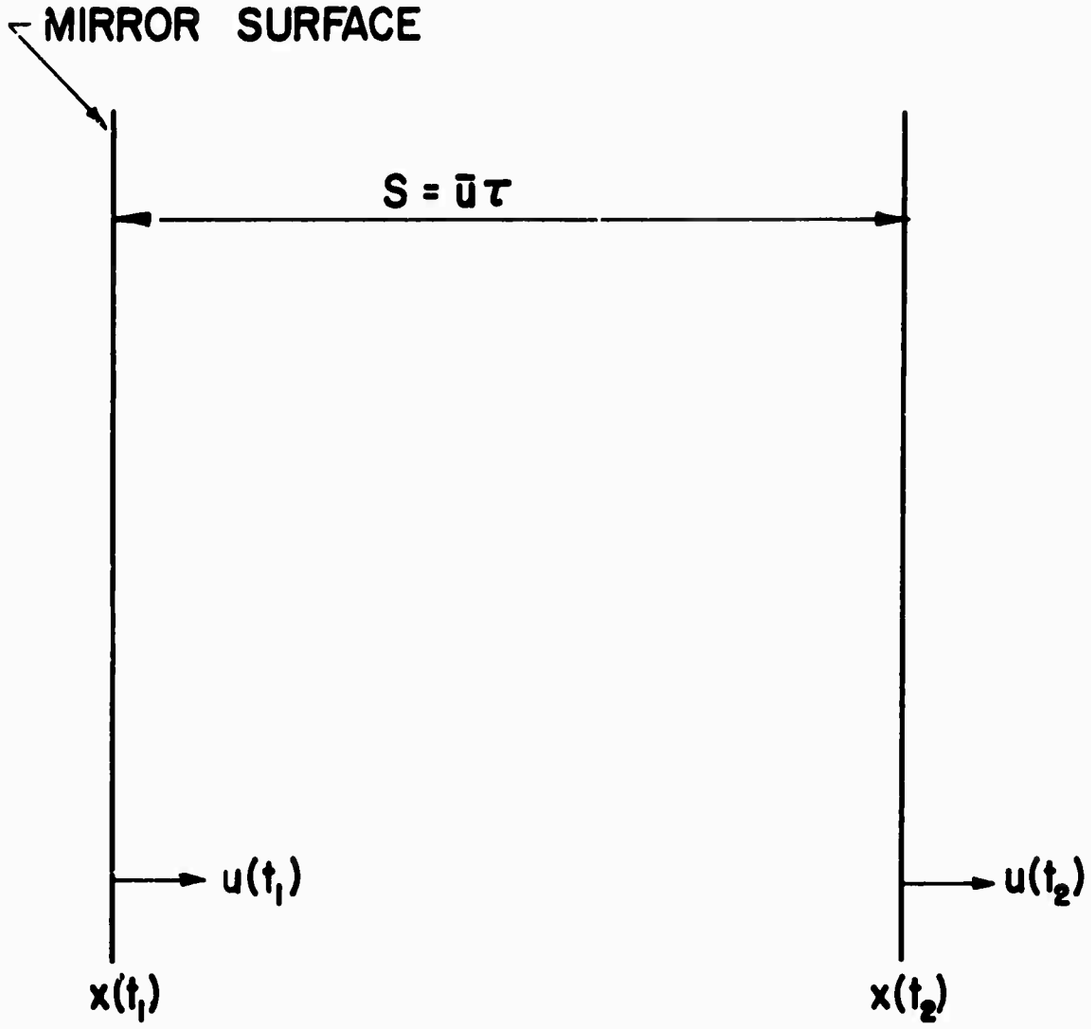

Figure 10. Diagram Showing Displacement of Target Surface during Delay Interval, τ (= $t_2 - t_1$).

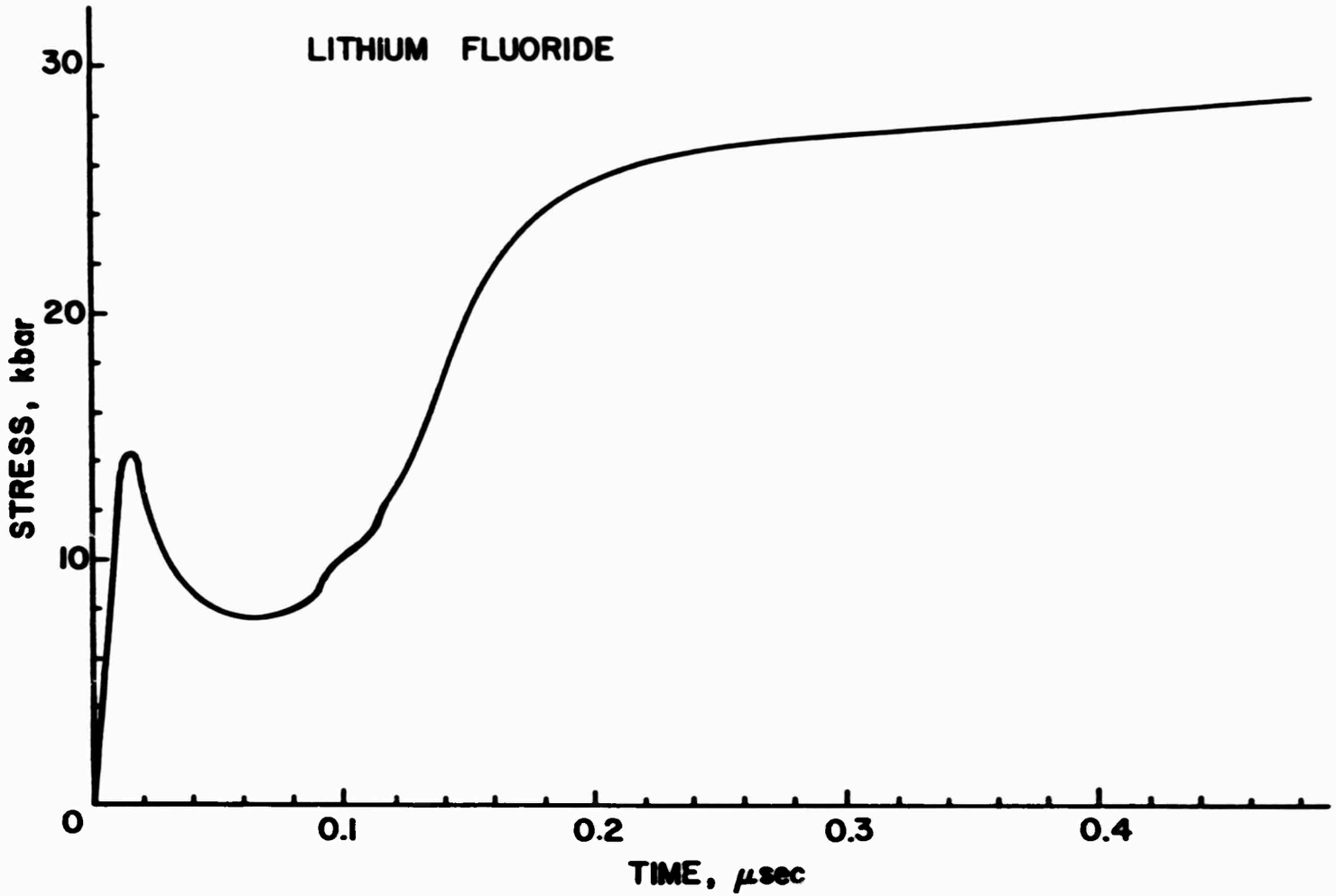

Figure 11. Quartz Gage Record of Compressive Portion of Stress Wave in LiF Crystal (001 orientation), Thickness 2.133 mm. Impact with Al projectile produced step stress pulse of 25 kbar in LiF. (After Asay[87])

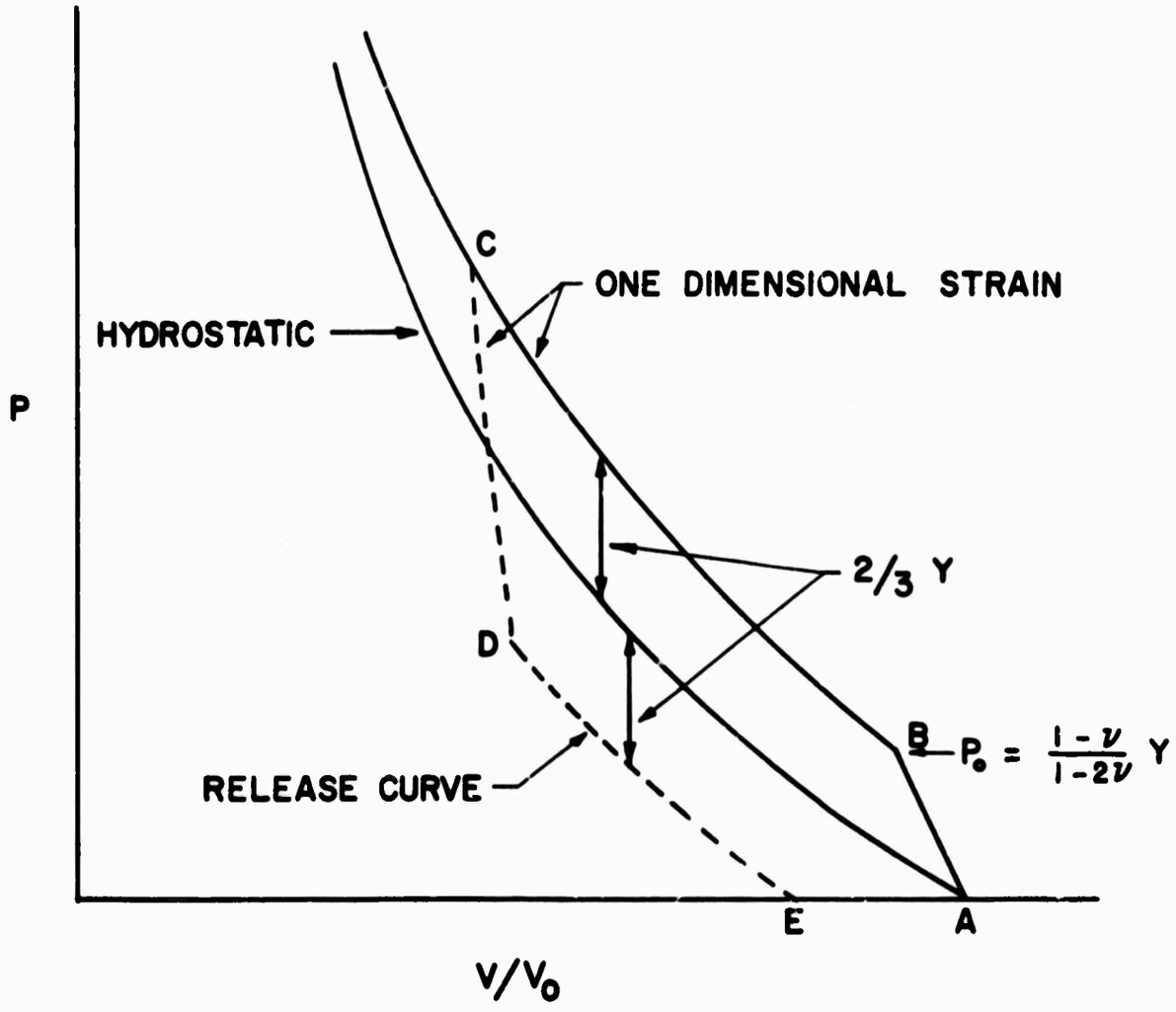

Figure 12. Stress-Volume Curves for One-Dimensional Strain Based on Elastic-Plastic Model. Relief of stress from a (shocked) state "C" follows path CDE. P_o is Hugoniot elastic limit, Y is yield stress.

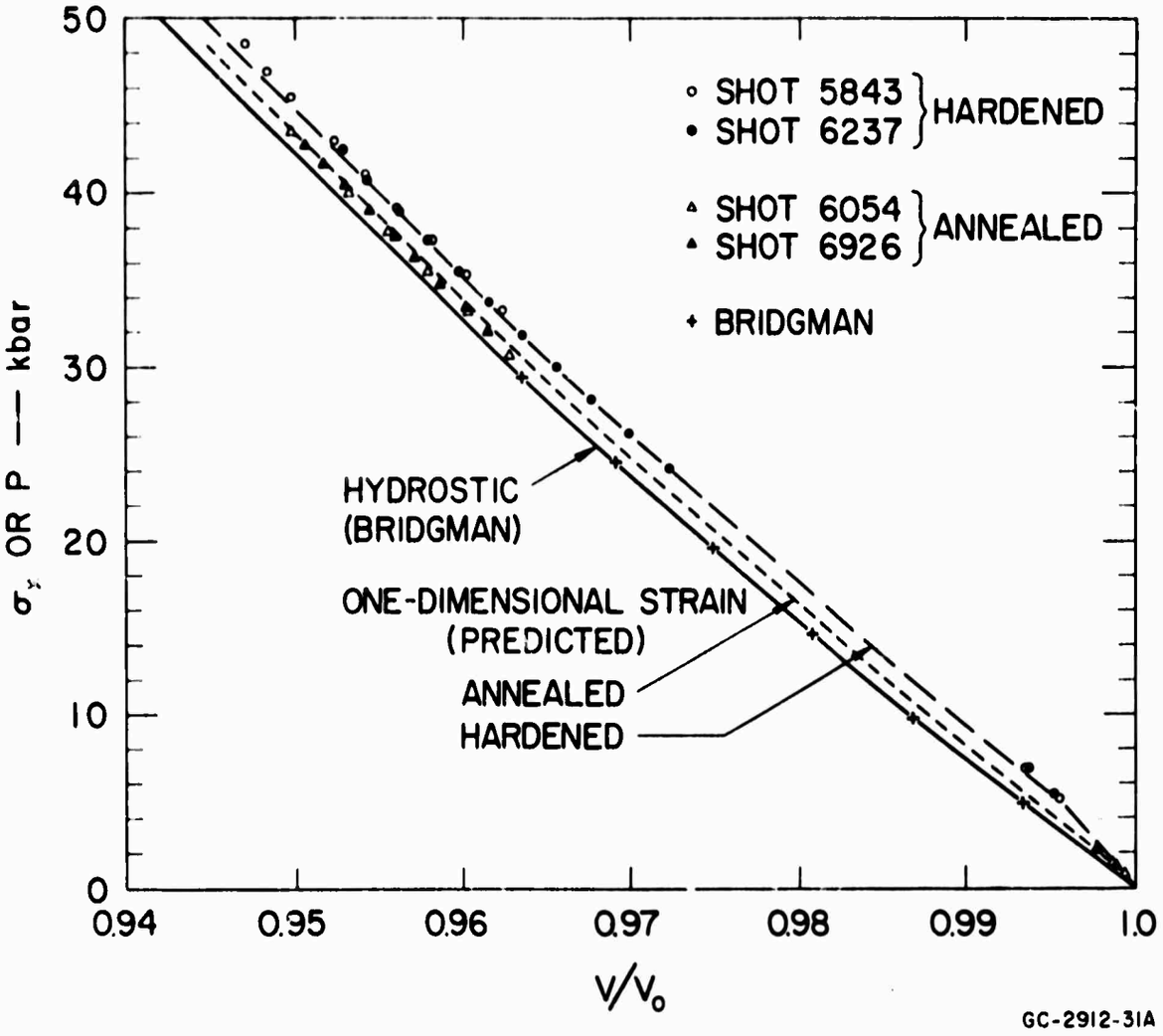

Figure 13. Comparison of Hugoniot and Hydrostatic Compression States in 2024 Aluminum.[11]

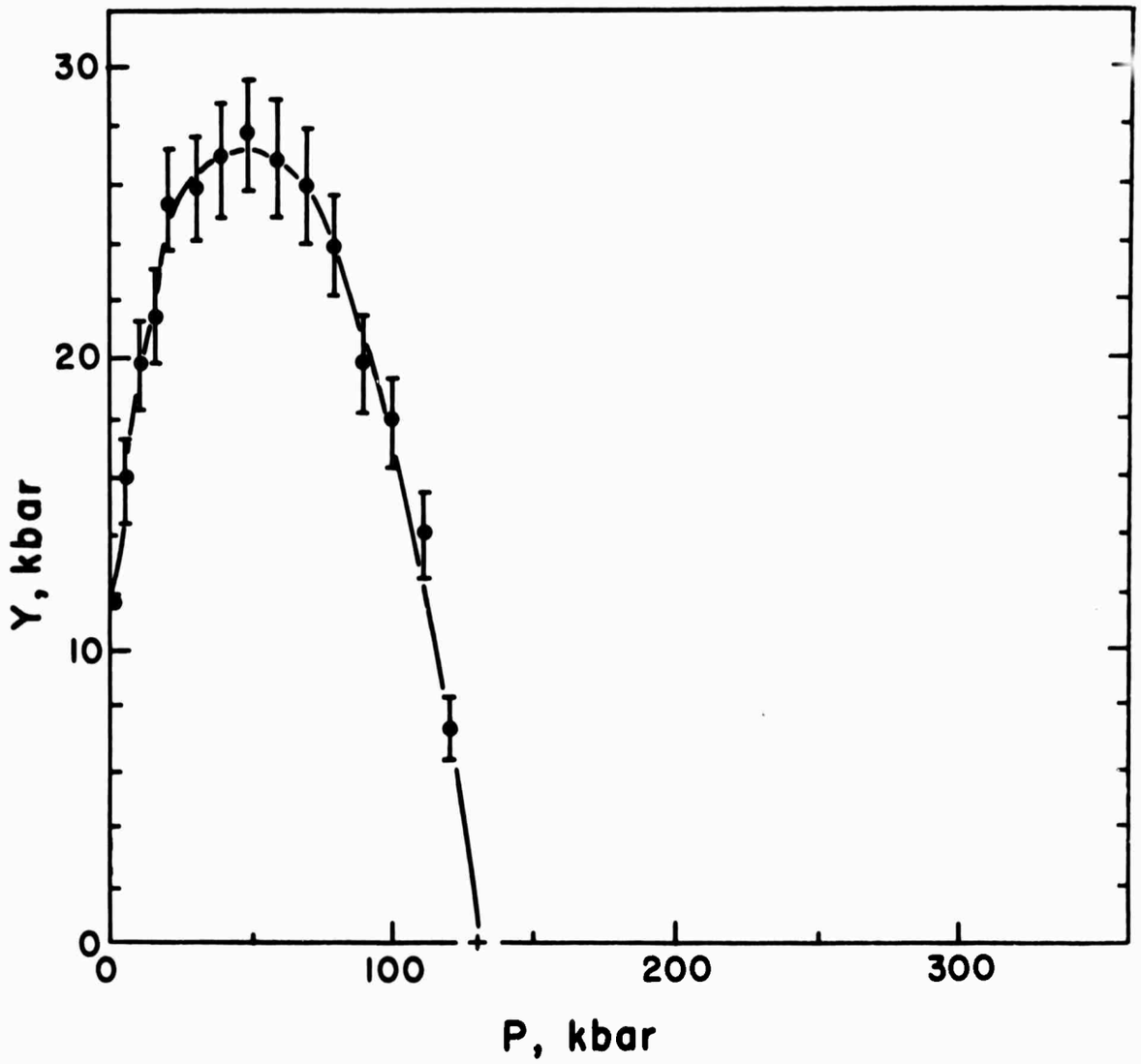

Figure 14. Yield Stress in 2024 Aluminum Shocked to 130 kbar. Values are determined from comparison of compression and relief states. (After van Thiel and Kusubov[28])

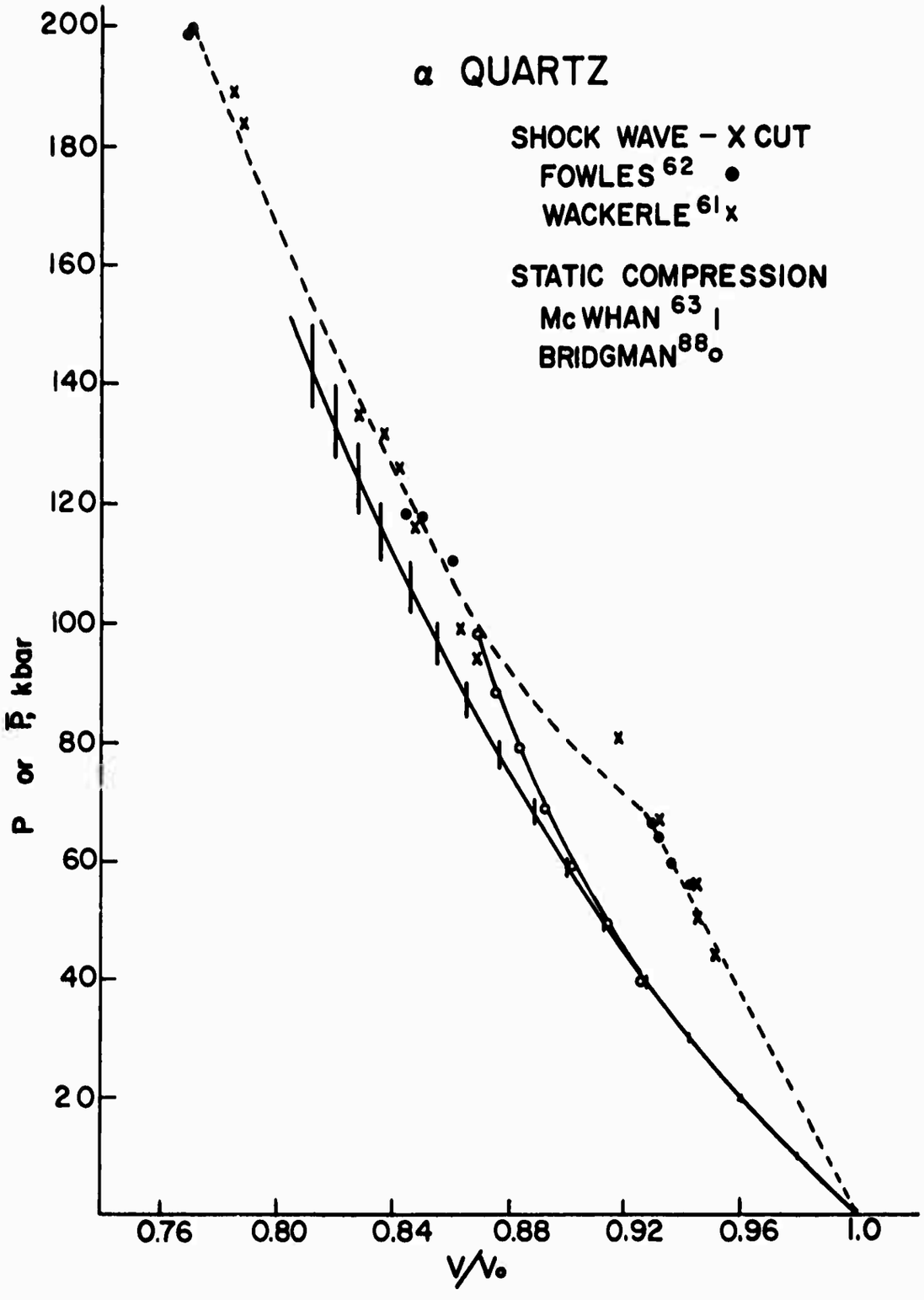

Figure 15. Comparison of Hydrostatic and Shocked States in α-quartz (x-cut).[61-63] Disparities in the hydrostatic curves cause uncertainties in the shear stress of the shocked state above 80 kbar.

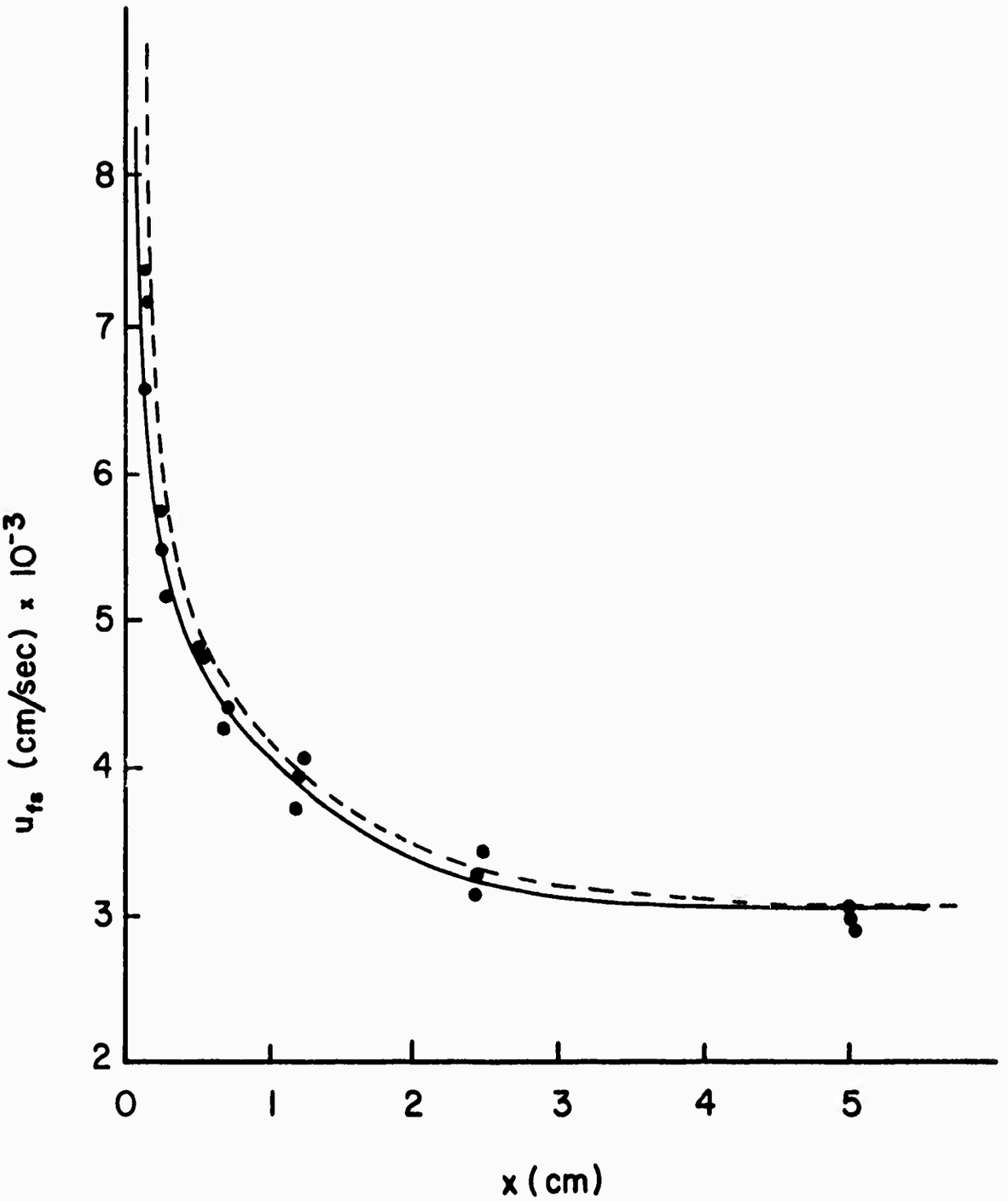

Figure 16. Decay of Precursor Amplitude in Armco Iron. Curves are fitted using Gilman dislocation velocity model. (After Taylor[40])

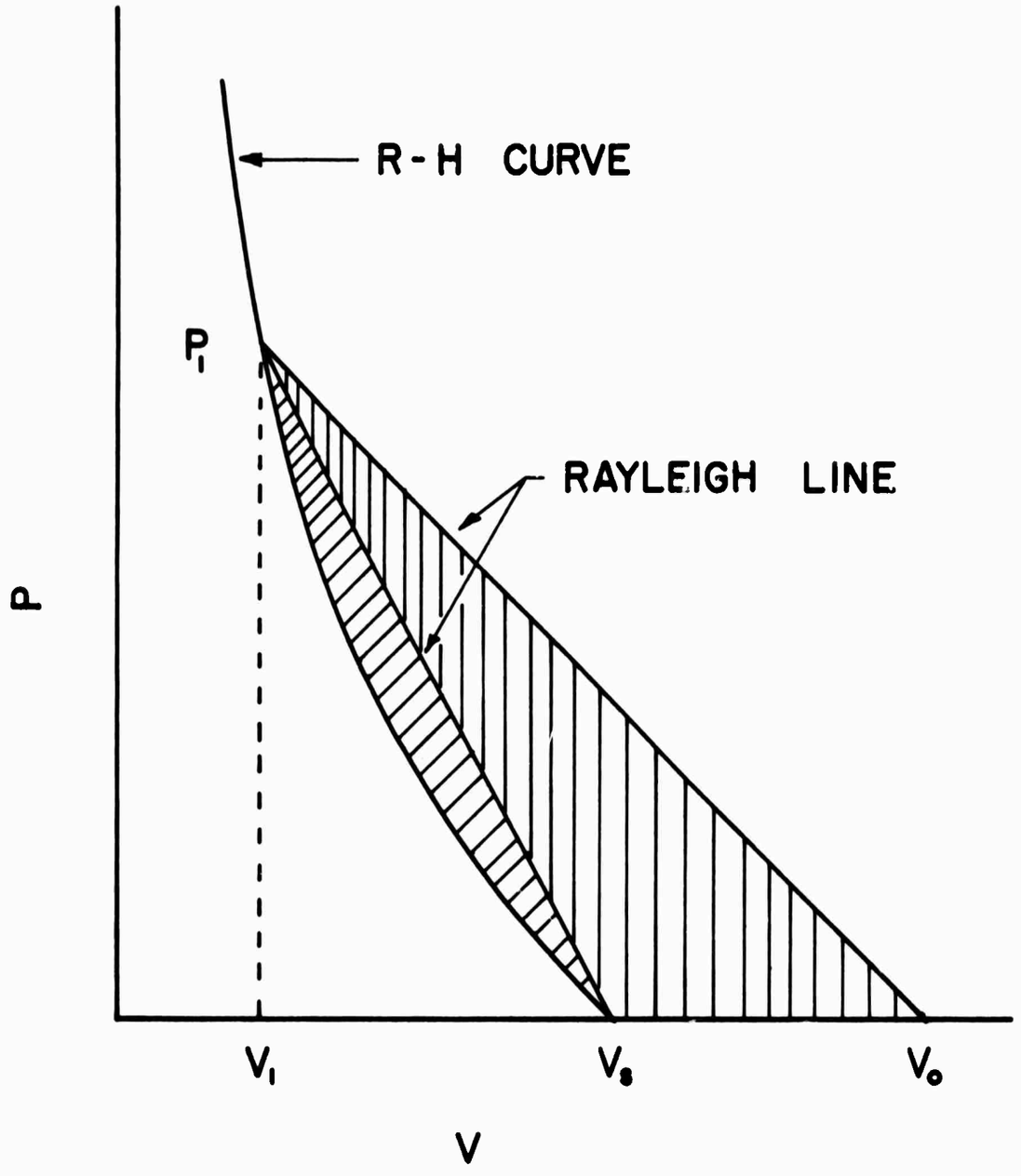

Figure 17. Approximate Hugoniot and Rayleigh Lines for Solid and Porous Material. Cross-hatched areas represent energy dissipated in shock transition.

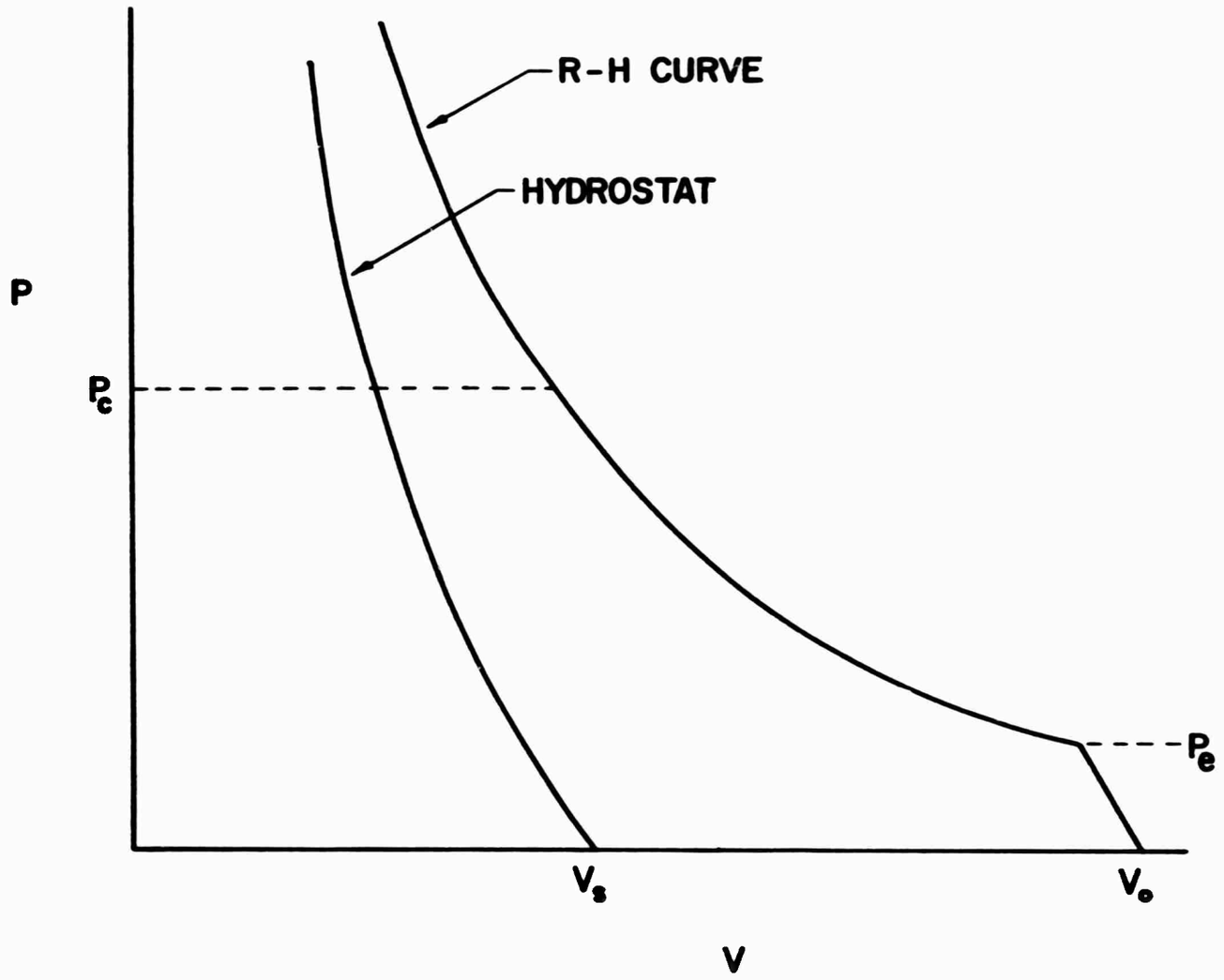

Figure 18. Comparison of R-H Curve of Porous Material with Hydrostat of Solid Showing Hugoniot Elastic Limit, Compaction Region and Stress Difference due to Shock Heating.

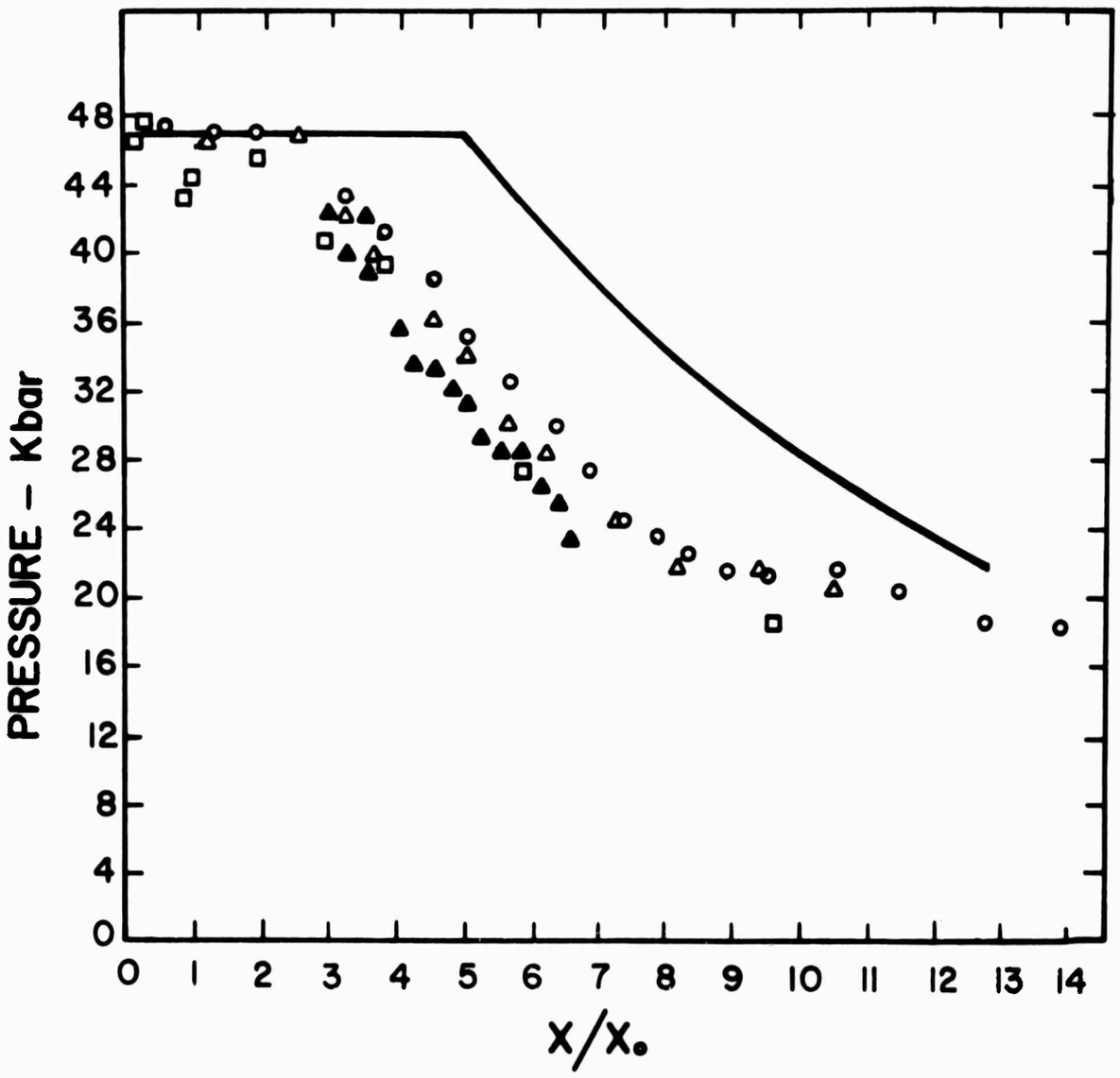

Figure 19. Decay of Peak Shock Stress with Propagation Distance in Epoxy. Solid curve is predicted on the basis of fluid model neglecting shear stresses. X_o is the thickness of the flyer plate that produced the shock. (After Erkman[58])

UNCLASSIFIED

Security Classification

20 JUL '70 (SRS)

DOCUMENT CONTROL DATA - R & D

(Security classification of title, body of abstract and indexing annotation must be entered when the overall report is classified)

1. ORIGINATING ACTIVITY *(Corporate author)*

Washington State University
Department of Physics
Pullman, Washington 99163

2a. REPORT SECURITY CLASSIFICATION

UNCLASSIFIED

2b. GROUP

3. REPORT TITLE

"DETERMINATION OF CONSTITUTIVE RELATIONS FROM PLANE WAVE EXPERIMENTS"

4. DESCRIPTIVE NOTES *(Type of report and inclusive dates)*

Scientific -----Interim

5. AUTHOR(S) *(First name, middle initial, last name)*

G. Richard Fowles

6. REPORT DATE	7a. TOTAL NO. OF PAGES	7b. NO. OF REFS
APR [illegible] 1970	74	88

8a. CONTRACT OR GRANT NO.	9a. ORIGINATOR'S REPORT NUMBER(S)
F44620-67-C-0087	
b. PROJECT NO. AO 985-3 (ARPA)	
c. 61102F	9b. OTHER REPORT NO(S) *(Any other numbers that may be assigned this report)* AFOSR 70-2022 TR
d. 681301	

10. DISTRIBUTION STATEMENT

This document has been approved for public release and resale; its distribution is unlimited

11. SUPPLEMENTARY NOTES	12. SPONSORING MILITARY ACTIVITY
PROCEEDINGS. Proceedings of Symposium 2, "Characteristics of the Dynamic Behavior of Materials"	Air Force Office of Scientific Research (SRS) 1400 Wilson Boulevard, Arlington Virginia 22209

13. ABSTRACT Albuquerque, NM, 25-27 Aug 69,

Recent developments in experimental methods for measuring the characteristics of plane compression waves are reviewed, and analytical methods for inferring constitutive relations from measured wave profiles are discussed. A general method, requiring only pressure or particle velocity measurements, is proposed that is applicable to arbitrary waves in which equilibrium or steady state may not obtain. A summary of current knowledge of constitutive relations obtained from plane wave experiments is also presented.

DD FORM 1 NOV 68 1473

UNCLASSIFIED

Security Classification